







Glycogen synthesis prevents metabolic imbalance and disruption of photosynthetic electron transport from photosystem II during transition to photomixotrophy in *Synechocystis* sp. PCC 6803

Pablo Ortega-Martínez^{1,2*} , Lauri Nikkanen^{3*} , Laura T. Wey³ , Francisco J. Florencio^{1,2} ,
Yagut Allahverdiyeva³  and Sandra Díaz-Troya^{1,2} 

¹Instituto de Bioquímica Vegetal y Fotosíntesis, Universidad de Sevilla, Consejo Superior de Investigaciones Científicas, Américo Vespucio 49, Sevilla, 41092, Spain; ²Departamento de Bioquímica Vegetal y Biología Molecular, Facultad de Biología, Universidad de Sevilla, Profesor García González s/n, Sevilla, 41012, Spain; ³Molecular Plant Biology, Department of Life Technologies, University of Turku, Turku, FI-20014, Finland

Summary

Authors for correspondence:
Sandra Díaz-Troya
Email: sdtroya@us.es

Yagut Allahverdiyeva
Email: allahve@utu.fi

Received: 13 February 2024
Accepted: 17 April 2024

New Phytologist (2024) **243**: 162–179
doi: 10.1111/nph.19793

Key words: cyanobacteria, glucose, glycogen, metabolism, mixotrophy, photomixotrophy, photosynthesis.

- Some cyanobacteria can grow photoautotrophically or photomixotrophically by using simultaneously CO₂ and glucose. The switch between these trophic modes and the role of glycogen, their main carbon storage macromolecule, was investigated.
- We analysed the effect of glucose addition on the physiology, metabolic and photosynthetic state of *Synechocystis* sp. PCC 6803 and mutants lacking phosphoglucomutase and ADP-glucose pyrophosphorylase, with limitations in glycogen synthesis.
- Glycogen acted as a metabolic buffer: glucose addition increased growth and glycogen reserves in the wild-type (WT), but arrested growth in the glycogen synthesis mutants. Already 30 min after glucose addition, metabolites from the Calvin–Benson–Bassham cycle and the oxidative pentose phosphate shunt increased threefold more in the glycogen synthesis mutants than the WT. These alterations substantially affected the photosynthetic performance of the glycogen synthesis mutants, as O₂ evolution and CO₂ uptake were both impaired.
- We conclude that glycogen synthesis is essential during transitions to photomixotrophy to avoid metabolic imbalance that induces inhibition of electron transfer from PSII and subsequently accumulation of reactive oxygen species, loss of PSII core proteins, and cell death. Our study lays foundations for optimising photomixotrophy-based biotechnologies through understanding the coordination of the crosstalk between photosynthetic electron transport and metabolism.

Introduction

The biosphere and trophic chains are sustained by photosynthetic organisms, including cyanobacteria, algae and plants. Photoautotrophic growth involves the fixation of CO₂ into metabolism through the Calvin–Benson–Bassham (CBB) cycle, fuelled by photosynthetic processes. Cyanobacteria are unique as prokaryotic oxygenic photosynthetic microorganisms and play a crucial role in the global carbon cycle, contributing *c.* 25% of annual global productivity (Field *et al.*, 1998). Additionally, cyanobacteria are increasingly used as green cell factories by redirecting their metabolism towards the biosynthesis of desired compounds. Besides photoautotrophic growth, some cyanobacteria such as *Synechocystis* sp. PCC 6803 (hereafter *Synechocystis*) have a plastic metabolic network that enables growth under a variety of trophic conditions, including photomixotrophy (Luan *et al.*, 2019;

Muth-Pawlak *et al.*, 2022). Under photomixotrophy, cells can supplement photosynthesis by using organic carbon compounds from the environment, such as glucose, sucrose, glycerol or acetate (Matson & Atsumi, 2018). The dual carbon source enhances growth, offering attractive possibilities for biotechnology (Wan *et al.*, 2015; Kanno *et al.*, 2017; Luan *et al.*, 2019). Despite their ecological and biotechnological significance (Muñoz-Marín *et al.*, 2024), the physiological mechanisms underlying the transition from photoautotrophy to photomixotrophy in cyanobacteria and the role of the main carbon storage macromolecule glycogen in that process remain poorly understood.

The CBB cycle is an energy-demanding process that requires both ATP and NADPH produced in the photosynthetic electron transport chain (PETC). Briefly, the photolysis of water by photosystem II (PSII) releases electrons as well as molecular oxygen (O₂) as a by-product (Fig. 1). In linear electron transfer (LET) these electrons ultimately reduce ferredoxin (Fd), which, in turn, is used to generate NADPH. The PETC generates a

*These authors contributed equally to this work.

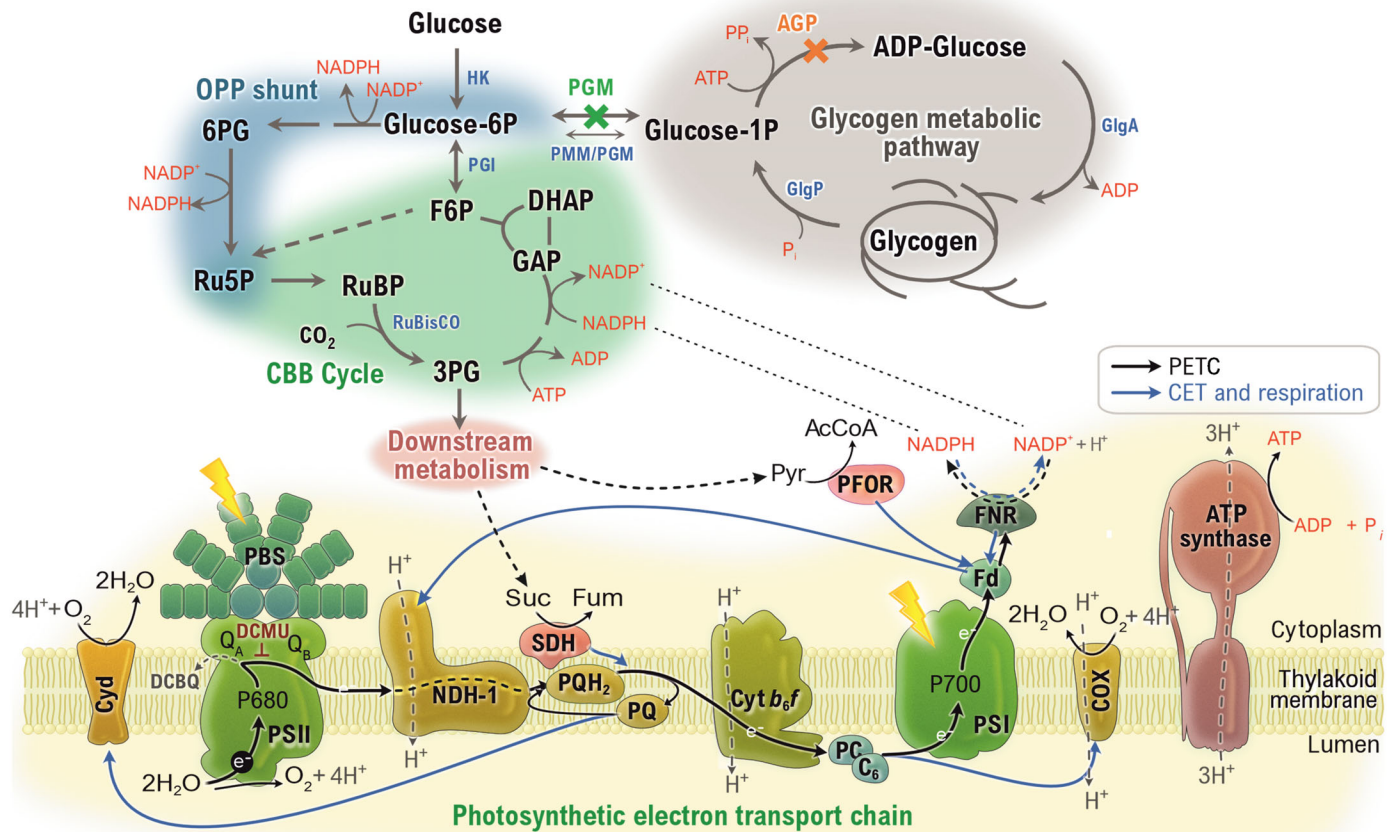


Fig. 1 Diagram of the main metabolic pathways and their interconnections to photosynthesis in *Synechocystis* sp. PCC 6803. Each route is colour-coded for clarity: the glycogen metabolic pathway (grey), the oxidative pentose phosphate (OPP) shunt (blue), the Calvin–Benson–Bassham (CBB) cycle (green), the photosynthetic electron transport chain (PETC, yellow), and the downstream metabolism of 3-phosphoglycerate (3PG, pink). The Entner–Doudoroff pathway, tricarboxylic acid cycle and flavodiiron proteins are not depicted. Glucose assimilation involves its phosphorylation to glucose-6P by hexokinase (HK), followed by conversion to either 6P-gluconate (6PG) through the action of glucose-6P dehydrogenase in the OPP shunt, or fructose-6P (F6P) via phosphoglucose isomerase (PGI) through the PGI shunt. Another route to G6P is its interconversion to glucose-1P by the phosphoglucomutases (PGM and PMM/PGM) and its incorporation to glycogen by the action of ADP-glucose pyrophosphorylase (AGP) and glycogen synthases (GlgAs) with ATP consumption. In the CBB cycle, CO₂ is incorporated into the intermediate metabolite ribulose 1,5-bisphosphate (RuBP) by RuBisCO releasing two molecules of 3-phosphoglycerate (3PG). Some 3PG is used for biosynthetic processes, while the majority is redirected to the CBB cycle to replenish the RuBP pools and ensure efficient CO₂ fixation. In this cycle, 3PG undergoes phosphorylation by 3-phosphoglycerate kinase and subsequent reduction by glyceraldehyde-3-phosphate dehydrogenase generating glyceraldehyde-3P (GAP), with the consumption of ATP and NADPH, respectively. The PETC consists of protein complexes that transport electrons through linear (LET, black arrows) or cyclic (CET, blue arrows) pathways: Within photosystem II (PSII) and photosystem I (PSI) the electrons are excited by photons harnessed by phycobilisome (PBS) antennae and Chls. Respiration (RET, blue arrows) also takes place in thylakoids. The green and orange crosses depicted on upper panel of the PGM and AGP reactions arrows represent the knock-out mutations used to study glycogen metabolism. *c*₆, cytochrome *c*₆; COX, cytochrome *c* oxidase; *cyd*, cytochrome *bd*-quinol oxidase; *Cyt b*₆*f*, cytochrome *b*₆*f*; DCMU, 2,6-Dichloro-1,4-benzoquinone; DCMU, 3-(3,4-dichlorophenyl)-1,1-dimethylurea; DHAP, Dihydroxyacetone-P; Fd, Ferredoxin; FNR, Ferredoxin-NADPH reductase; Fum, Fumarate; NDH-1, NADPH dehydrogenase complexes; OEC, oxygen-evolving complex; PC, plastocyanin; PFOR, Pyruvate-Ferredoxin oxidoreductase; PQ/PQH₂, plastoquinone pool; PSI, photosystem I; PSII, photosystem II; Ru5P, Ribulose-5P; RuBisCO, Ribulose-1,5-P Carboxylase Oxidase; SDH, succinate dehydrogenase; Suc, Succinate.

proton motive force (*pmf*) over the thylakoid membrane through different mechanisms, such as water oxidation and proton translocation associated with the plastoquinone (PQ) reductive cycle. Other complexes, such as NAD(P)H dehydrogenase-like (NDH-1) complex and the respiratory terminal oxidase COX, also contribute to proton gradient formation. The *pmf* is harnessed by ATP synthase to produce ATP. The electrons from Fd can also

be diverted back to the PETC in cyclic electron transfer (CET), facilitating *pmf* generation. Cells can adjust the rates of LET and CET based on their energetic requirements for the ATP/NADPH ratio under variable environmental conditions (Nikkanen *et al.*, 2021; Theune *et al.*, 2021; Miller *et al.*, 2022). In contrast to photosynthetic eukaryotes, which perform catabolic and anabolic reactions in separate organelles, cyanobacteria partly

share the PETC for respiration (Fig. 1, Mullineaux, 2014; Lea-Smith *et al.*, 2016).

Exogenous organic compounds such as glucose are incorporated via membrane transporters, imposing reorganisations of several metabolic processes, the details of which remain unclear (Kahlon *et al.*, 2006; Trautmann *et al.*, 2012; Burnap *et al.*, 2015; Zavřel *et al.*, 2017). First, sharing PETC components, such as the PQ pool, cytochrome (Cyt) *b₆f* complex, plastocyanin (PC) or Cyt *c₆* between photosynthesis and respiration requires adjustments to fulfil cellular demands while preventing overreduction (Mullineaux, 2014). Second, glucose supplementation rearranges metabolism to optimise resource utilisation. For example, fluxomic studies have revealed that carbon metabolic flux is largely redirected towards increasing ribulose-1,5-bisphosphate carboxylase/oxygenase (RuBisCO) activity, thus boosting CO₂ fixation in the CBB cycle (Schulze *et al.*, 2022). The remaining carbon is predominantly channelled to glycogen, which serves as a carbon and energy buffer and plays a crucial role in the plasticity of cell metabolism (Cano *et al.*, 2018; Luan *et al.*, 2019; Makowka *et al.*, 2020; Ortega-Martínez *et al.*, 2023).

Glycogen is synthesised from ADP-glucose in a pathway widely conserved in bacteria (Fig. 1). ADP-glucose synthesis requires G1P, which is produced in a bidirectional reaction using glucose-6P (G6P) by the phosphohexomutase enzymes, such as phosphoglucomutase (PGM), and to a lesser extent by phosphomannomutase/phosphoglucomutase (PMM/PGM). G1P is then coupled with ATP to produce ADP-glucose by ADP-glucose pyrophosphorylase (AGP), which is used by glycogen synthase(s) (GlgA) to elongate the glycogen chains (Ball & Morell, 2003; Cifuentes *et al.*, 2019). Strains deficient in either AGP or PGM, which contain null or reduced glycogen levels, respectively, are viable under permissive conditions (Gründel *et al.*, 2012; Doello *et al.*, 2022; Ortega-Martínez *et al.*, 2023).

However, under stress conditions, such as high light intensity, nitrogen deprivation or extended darkness, they exhibit impaired growth, metabolic overflow, and cell death (Carrieri *et al.*, 2012; Cano *et al.*, 2018; Ortega-Martínez *et al.*, 2023). Furthermore, the sensitivity of glycogen-less *Synechocystis* mutants to photomixotrophic conditions (Gründel *et al.*, 2012) suggests that glycogen is crucial in the transition between trophic modes.

In this study we investigated the photosynthetic and metabolic response of *Synechocystis* during transitions from photoautotrophy to photomixotrophy. We aimed to understand how the ability to store excess carbon in glycogen influences these responses. Towards these aims, we analysed glycogen synthesis mutant strains ΔPGM and ΔAGP using metabolomics and a suite of biophysical and biochemical techniques to study photosynthesis. We found that in glycogen synthesis mutants, the presence of an organic carbon source caused accumulation of most metabolites in the intertwined pathways of central carbon metabolism, as well as a swift decline in photosynthetic electron transport due to restriction of electron transfer from PSII. Our study provides valuable physiological insights into the metabolic transition from photoautotrophic to photomixotrophic conditions, shedding light on the mechanisms of

coordinating the intertwined bioenergetics of photosynthesis and metabolism.

Materials and Methods

Strains and culture conditions

Glucose-tolerant WT strain of *Synechocystis* sp. PCC 6803 and mutants in phosphoglucomutase (PGM) (Δpgm::CK1, Ortega-Martínez *et al.*, 2023) and ADP-glucose pyrophosphorylase (AGP) (Δagp::C.C1, Díaz-Troya *et al.*, 2014) were cultivated in either BG11 buffered to pH 7.5 with 20 mM HEPES-KOH (BG11) or BG11 with 12 mM bicarbonate (BG11C) (Rippka *et al.*, 1979). No differences were observed in growth and oxygen evolution rates between media.

Cell growth was monitored by OD_{750 nm}. Precultures in mid-logarithmic phase grown at 30°C under constant light at 40 ± 5 μmol photons m⁻² s⁻¹, and with continuous shaking at 100 rpm under atmospheric CO₂ were adjusted to 0.8 OD_{750 nm} 24 h before the experiments. On the day of the experiment, cultures were centrifuged, resuspended in fresh medium at 1 OD_{750 nm} or at the Chl concentration described for each experiment. WT, ΔPGM and ΔAGP cultures adjusted to 1 OD_{750 nm} had Chl contents of 4.68 ± 0.46, 4.95 ± 0.38 and 4.79 ± 0.48 (mean ± SD) μg Chl ml⁻¹, respectively. Cultures were then acclimated to the same growth conditions described above for 2 h before adding 2 mM glucose (Acros Organics, Geel, Belgium).

Glycogen content and glucose consumption determination

Glycogen was purified and digested to glucose as described in Ortega-Martínez *et al.* (2023). Glucose derived from purified glycogen and glucose content in the media were measured using a colorimetric assay based on the oxidation of 200 mg ml⁻¹ of O-Dianisidine (Sigma) by 5 U ml⁻¹ of peroxidase (from horseradish, Sigma) using the H₂O₂ released from glucose by 25 U ml⁻¹ glucose oxidase (from *Aspergillus niger*, Sigma) for 30 min at 37°C. The reaction was quenched by adding H₂SO₄ to a final concentration of 4.8 N, and absorbance was measured at 540 nm using a Varioskan multiplate reader (Thermo Fisher Scientific, Erlangen, Germany). Standard curves of known amounts of amyloglucosidase-digested glycogen or glucose were employed for quantification.

Protein extraction and immunoblotting

Ten milliliter cultures were harvested and frozen at -20°C. Pellets were resuspended in 50 mM Tris-HCl (pH 8), 25 mM NaCl, and 1 mM phenylmethylsulphonyl fluoride (PMFS) with glass beads. Cells were lysed by mechanical disruption at 6 m s⁻¹ for 30 s in a FastPrep-24 5G (MP Biomedicals, Santa Ana, CA, USA). Tubes were centrifuged at 4°C for 5 min at 1500 g and supernatants collected. Total protein content was determined a Lowry assay (Markwell *et al.*, 1978).

Fifteen micrograms of protein was resolved by SDS-PAGE (10% acrylamide/bis-acrylamide) containing 6 M urea and

transferred to a polyvinylidene difluoride membrane (Immobilon-P; Millipore). Blocking, probing and detection was performed as in Ortega-Martínez *et al.* (2023) using primary antibodies against D1 (1 : 10 000, AS111786; Agrisera, Vännäs, Sweden) CP-47 (1 : 10 000, AS04038; Agrisera), PsaB (1 : 10 000, AS10695; Agrisera), ATP β (1 : 10 000, AS05085; Agrisera) or GroEL (1 : 75 000, G6532; Sigma-Aldrich) diluted in blocking solution.

Reactive oxygen species measurement

Reactive oxygen species levels were measured as outlined in Lee *et al.* (2018) with the following modifications. Samples were centrifuged at 10 000 *g* for 5 min. Pellets were resuspended in 0.8 ml of 1 \times phosphate-buffered saline (PBS) containing 50 μ M of the fluorescent probe 2',7'-dichlorofluorescein diacetate (DCFH-DA, D6883 Sigma-Aldrich). Samples were incubated for 1 h in darkness at 30°C with agitation. To eliminate free DCFH-DA, the samples were centrifuged at 10 000 *g* for 5 min and washed once with PBS. Cells were resuspended in 200 μ l PBS and transferred to a fluorescent 96-well microplate. Fluorescence of dichlorofluorescein (DCF), the oxidised form of DCFH, was measured at 525 nm after excitation at 488 nm in a Varioskan multiplate reader.

Glutathione pools quantification

Glutathione extraction and quantification was performed as outlined in Mallen-Ponce *et al.* (2022) using 10 ml culture harvested (5000 *g*, 5 min, 4°C) at the indicated times. Standards with known glutathione concentrations were used for quantification.

Targeted metabolomics (LC/MS)

Extraction and analysis of intracellular metabolites was performed using 2 OD_{750 nm} culture as described in Ortega-Martínez *et al.* (2023). For quantification of the total amount of metabolites, known concentrations of standards were used. Metabolites with concentration values outside the standard curve or not available for quantification are reported as fold change in relation to the WT value at the initial time point.

Gas exchange measurements

Real-time gas fluxes were measured from intact cells at a concentration of 10 μ g Chl ml⁻¹ under 50 μ mol photons m⁻² s⁻¹ of white actinic light using membrane inlet mass spectrometry (MIMS) as described in Solymosi *et al.* (2020). Cultures were first dark-adapted for 20 min, purged with N₂, and supplemented with 1.5 mM NaHCO₃ and ¹⁸O₂ at an equivalent concentration to ¹⁶O₂, enabling the differentiation of O₂ uptake from O₂ evolution. Gas exchange rates were calculated according to (Beckmann *et al.*, 2009). After 15 min of recording 0.5 mM 2,6-Dichloro-1,4-benzoquinone (DCBQ) in dimethyl sulfoxide (DMSO) was introduced into the sample chamber and measurements continued for 10 min.

Spectrometry

Chlorophyll fluorometry Induction curves of Chl fluorescence from intact cells were measured using a DUAL-PAM-100 fluorometer as outlined in Ortega-Martínez *et al.* (2023). Cells at 5 μ g Chl ml⁻¹ and dark-adapted for 10 min were exposed to red actinic light at 40 μ mol photons m⁻² s⁻¹ and multiple saturating pulses, followed by a postillumination recovery.

Reoxidation kinetics of Q_A⁻ The relaxation kinetics of single-turnover flash-induced Chl fluorescence were monitored using an FL 3500 fluorometer (PSI Instruments, Drásov, Czech Republic). Cells were adjusted to 7.5 μ g Chl ml⁻¹ and dark-adapted for 10 min before measurements. Measurements were performed with or without 10 μ M 3-(3,4-dichlorophenyl)-1,1-dimethylurea (DCMU). Curves were baselined to the fluorescence before the flash and normalised to the maximum fluorescence after the flash. The fluorescence decay traces were fitted to a three-component exponential decay function ($y = A1^{(-x/\tau1)} + A2^{(-x/\tau2)} + A3^{(-x/\tau3)} + y_0$) using ORIGINPRO 2023b.

PC, P700 and Fd redox changes Redox changes of PC, P700 and Fd in cells adjusted to 20 μ g Chl ml⁻¹ were obtained by NIR absorption difference spectrometry using a DUAL-KLAS-NIR spectrophotometer (Walz) and a NIRMAL script modified for cyanobacteria (3 s AL with a MT at 200 ms to obtain maximal values of Fd reduction and PC and P700 oxidation) (Schreiber & Klughammer, 2016). The model spectra for deconvolution of *Synechocystis* PC, P700, and Fd signals were measured as in Nikkanen *et al.* (2020).

LET and CET quantification The rates of LET and CET through PSI were quantified using analysis of dark interval relaxation kinetics (DIRK) in the absence or presence of 10 μ M DCMU as described in Theune *et al.* (2021). Cells were preilluminated for 2 min under 50 μ mol photons m⁻² s⁻¹ and subjected to 100 dark intervals of 20 ms with 1 s illumination between each repetition. Traces from all 100 dark intervals were then averaged.

Cytochrome *b₆f* redox kinetics Cytochrome *f* and *b* heme redox kinetics were measured as described in Solymosi *et al.* (2020) using a JTS-10 spectrophotometer (BioLogic).

NAD(P)H fluorescence Light-induced NAD(P)H redox kinetics were measured from 7.5 μ g Chl ml⁻¹ samples at 30°C, monitoring fluorescence changes between 420 and 580 nm after excitation at 365 nm using the NADPH/9-AA module of a DUAL-PAM (Walz, Germany) (Nikkanen *et al.*, 2020).

Results

Glucose causes growth arrest, oxidative stress, and decrease in PSII levels in strains with impaired glycogen metabolism

To understand the role of glycogen metabolism during the transition to photomixotrophic conditions, we analysed the effect of

2 mM glucose addition to photoautotrophically grown cultures of a WT *Synechocystis* strain and mutants lacking either PGM or AGP, which exhibit reduced or no glycogen synthesis, respectively (Ortega-Martínez *et al.*, 2023, Fig. 2c).

WT cells transitioned to photomixotrophic conditions displayed sixfold higher increase in OD_{750 nm} than cells kept under photoautotrophic conditions within the first 4 h (Fig. 2a,b). Concomitantly, glycogen rapidly accumulated, reaching levels in 4 h that exceeded those in photoautotrophic cultures after 24 h by > 50% (Fig. 2c). Enhanced growth and glycogen synthesis were accompanied by complete consumption of the provided glucose within 24 h (Fig. 2d).

By contrast, in Δ PGM and Δ AGP cultures, the addition of glucose induced an immediate growth arrest (Fig. 2b) and pigmentation bleaching within 48 h (Fig. 2a). Minimal glucose consumption was observed, with over 75% and 90% of the initial amounts remaining in the media after 24 h for Δ PGM and Δ AGP, respectively (Fig. 2d). The Δ PGM mutant showed reduced amounts of glycogen, reaching < 20% of WT levels after 24 h, in both photomixotrophy and photoautotrophy (Fig. 2c). Glycogen was undetectable in the Δ AGP mutant, regardless of the availability of glucose in the medium (Fig. 2c).

We measured the activities of hexokinase (HK) and other enzymes involved in the glucose-6P intersection, such as phosphoglucosyltransferase (PGM), phosphoglucose isomerase (PGI) and glucose-6P dehydrogenase (G6PDH), to test if differences in glucose consumption rates between strains were caused by inactivity (Supporting Information Methods S1). The activity of these enzymes in cell extracts was similar between all strains (except for the absence of PGM activity in Δ PGM) and remained unchanged 4 h after glucose addition in all strains (Fig. S1).

The progressive bleaching observed in both mutant cultures (Fig. 2a) prompted us to assess the relative levels of PSII, photosystem I (PSI), and ATP synthase by immunoblotting. Initially, there were no significant changes in the levels of the proteins examined during the first 4 h. However, while WT maintained similar protein levels, the abundance of D1 and CP47 PSII core proteins decreased 75–80% in the glycogen synthesis mutant strains between four and 24 h after glucose addition (Figs 2e, S2). The level of the PSI core protein PsaB decreased by 20% in Δ PGM and by 50% in Δ AGP between four and 24 h (Fig. 2e). ATP β (or GroEL, probed as a housekeeping protein) levels did not change in the mutants after glucose addition (Fig. 2e). A lower accumulation of photosystem proteins in the mutants upon a shift to photomixotrophy could possibly be linked to the generation of reactive oxygen species (ROS) (Johnson & Pakrasi, 2022).

In vivo monitoring of ROS levels, using the probe 2',7'-dichlorofluorescein diacetate (DCFH-DA) demonstrated elevated ROS by a four- and sixfold in Δ PGM and Δ AGP mutants, respectively, after 24 h under photomixotrophy (Fig. 2f). To investigate the role of oxidative stress protection upon a shift to photomixotrophy, we measured the *in vivo* levels of the key ROS scavenger glutathione using LC-MS. We detected similar glutathione pool sizes for all the strains in the absence of glucose (Fig. 2g). Upon the addition of glucose, WT cells gradually

increased their glutathione pool size, indicating an oxidative protective response. Contrarily, the glycogen synthesis mutants emptied their glutathione pools by 24 h (Fig. 2g). Removing glucose from the photomixotrophic mutant cultures 4 h postglucose addition prevented the adverse effects of glucose on the fitness of the cultures. However, after 24 h of glucose exposure, the mutant strains could not be recovered (Fig. S3).

Management of glucose-induced immediate metabolic alterations requires glycogen metabolism

To dissect the metabolic responses of WT and glycogen synthesis mutant cells during transitions to photomixotrophy, we employed targeted metabolomics to monitor the key carbon pathways, including the OPP shunt, the CBB cycle, the Entner–Meyerhof–Parnas (EMP) pathway that shares some intermediates with the CBB cycle, and the tricarboxylic acid (TCA) cycle, as well as the pool sizes of detectable amino acids (Figs 3, 4, S4; Dataset S1).

Before glucose addition (0 min), all strains presented similar levels of most examined metabolites, indicating that glycogen deficiency did not lead to major metabolic alterations under photoautotrophic conditions (Figs 3, 4, S4). Glucose addition induced rapid alteration in the levels of nearly all metabolites in all strains, with detectable changes already 5 min after glucose addition.

In WT, two distinct patterns of metabolic changes were observed (Figs 3, 4, S4). First, levels of the RuBisCO substrate ribulose-1,5-BP (RuBP), some of the metabolites shared by the CBB cycle and the EMP pathway (e.g. fructose-1,6-BP (F1,6BP), dihydroxyacetone-P (DHAP), 3PG), the last steps of the EMP pathway (e.g. phosphoenolpyruvate (PEP), pyruvate), and most TCA cycle intermediates underwent transient fluctuations, peaking 5–15 min after glucose addition (Figs 3, 4, S4a). These metabolites typically more than doubled their initial amounts before returning to photoautotrophic levels. Amino acids alanine and serine, derived from pyruvate and 3PG, respectively, increased more than fivefold, similarly to threonine and valine. Second, levels of metabolites from the OPP shunt (e.g. G6P, 6P-gluconate (6PG)), those from the CBB cycle (e.g. erythrose-4P (E4P) and sedoheptulose-7P (S7P)) and others in the interconnection of this cycle and the gluconeogenic EMP pathway (e.g. glyceraldehyde-3P (GAP), fructose-6P (F6P)) increased linearly three- to fivefold until 120 min (Figs 3, S4a).

In the glycogen synthesis mutants, glucose addition induced faster and more pronounced intermediate accumulation than in WT (Figs 3, 4, S4b). The first metabolites involved in glucose assimilation (G6P, 6PG, F6P) through the OPP shunt and PGI shunt increased rapidly and dramatically (by 5 min more than 40-, 10-, and 25-fold, respectively). This increase is key to enhance CO₂ fixation by providing CBB cycle intermediates under photomixotrophy (Schulze *et al.*, 2022). G1P, the first metabolite in the glycogen synthesis pathway, steadily increased by up to 10-fold in Δ AGP mutant but remained at low levels in Δ PGM, due to limited G6P/G1P interconversion in that mutant (Fig. S1, Ortega-Martínez *et al.*, 2023).

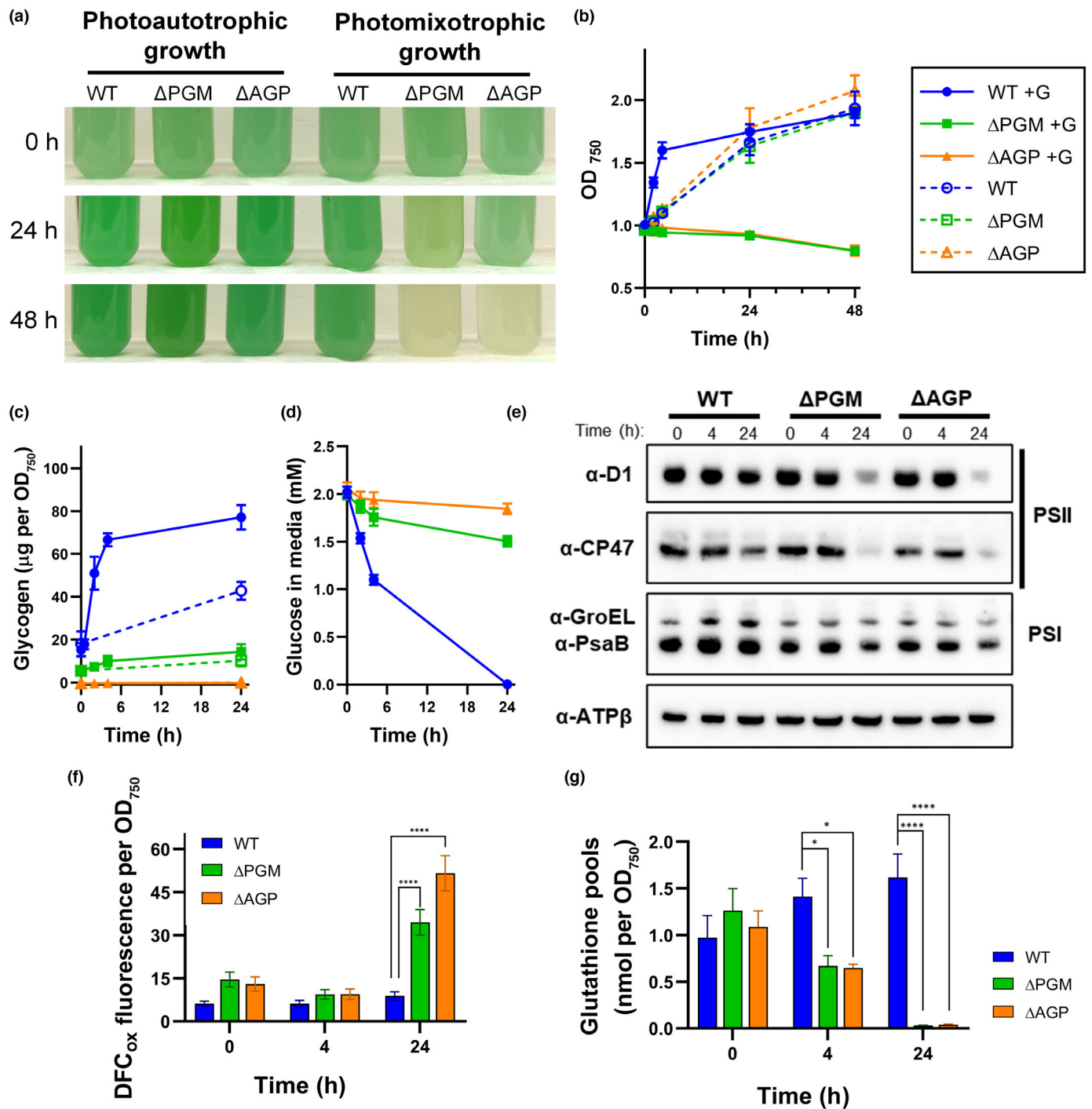


Fig. 2 Phenotypic characterisation of WT *Synechocystis* and strains with deficient glycogen metabolism after 2 mM glucose supplementation. Cultures grown under photoautotrophic conditions in BG11C were adjusted to a final optical density of 1 at 750 nm ($OD_{750\text{ nm}}$), divided into two flasks, and supplemented (photomixotrophy) or not (photoautotrophy) with 2 mM glucose. (a) Photographs of WT, Δ PGM and Δ AGP strains cultivated in parallel under either photoautotrophic or photomixotrophic conditions for 48 h. (b) Growth curves of WT, Δ PGM and Δ AGP strains measured as $OD_{750\text{ nm}}$ in both photoautotrophy (control, dash lines) and photomixotrophy (solid lines). (c) Time course glycogen content per optical density ($OD_{750\text{ nm}}$) of WT, Δ PGM and Δ AGP strains in the presence (solid lines) or absence (dashed lines) of glucose. (d) Glucose concentration in the media for 24 h after the initial addition of 2 mM of glucose. (e). Western blot analysis of proteins from the PETC (D1 and CP47 proteins of PSII and PsaB of PSI) and ATP synthase (ATP β , β subunit of ATP synthase) in the WT, Δ PGM and Δ AGP strains at 0, 4 and 24 h after glucose addition. A representative western blot of six biological replicates is shown. Quantifications of band intensity of all blots are shown in Supporting Information Fig. S2. (f) Quantification of cellular reactive oxygen species (ROS) accumulation measured by DFC fluorescence in the WT, Δ PGM and Δ AGP strains at 0, 4 and 24 h after glucose addition. (g) Quantification of glutathione pools in the WT, Δ PGM and Δ AGP strains at 0, 4 and 24 h after glucose addition. The data represent the mean \pm SE from six (c–e), five (f) and three (g) biological replicates, respectively. Statistical significance levels are denoted by *, $P < 0.05$; ****, $P < 0.0001$; otherwise, not significant (two-way ANOVA).

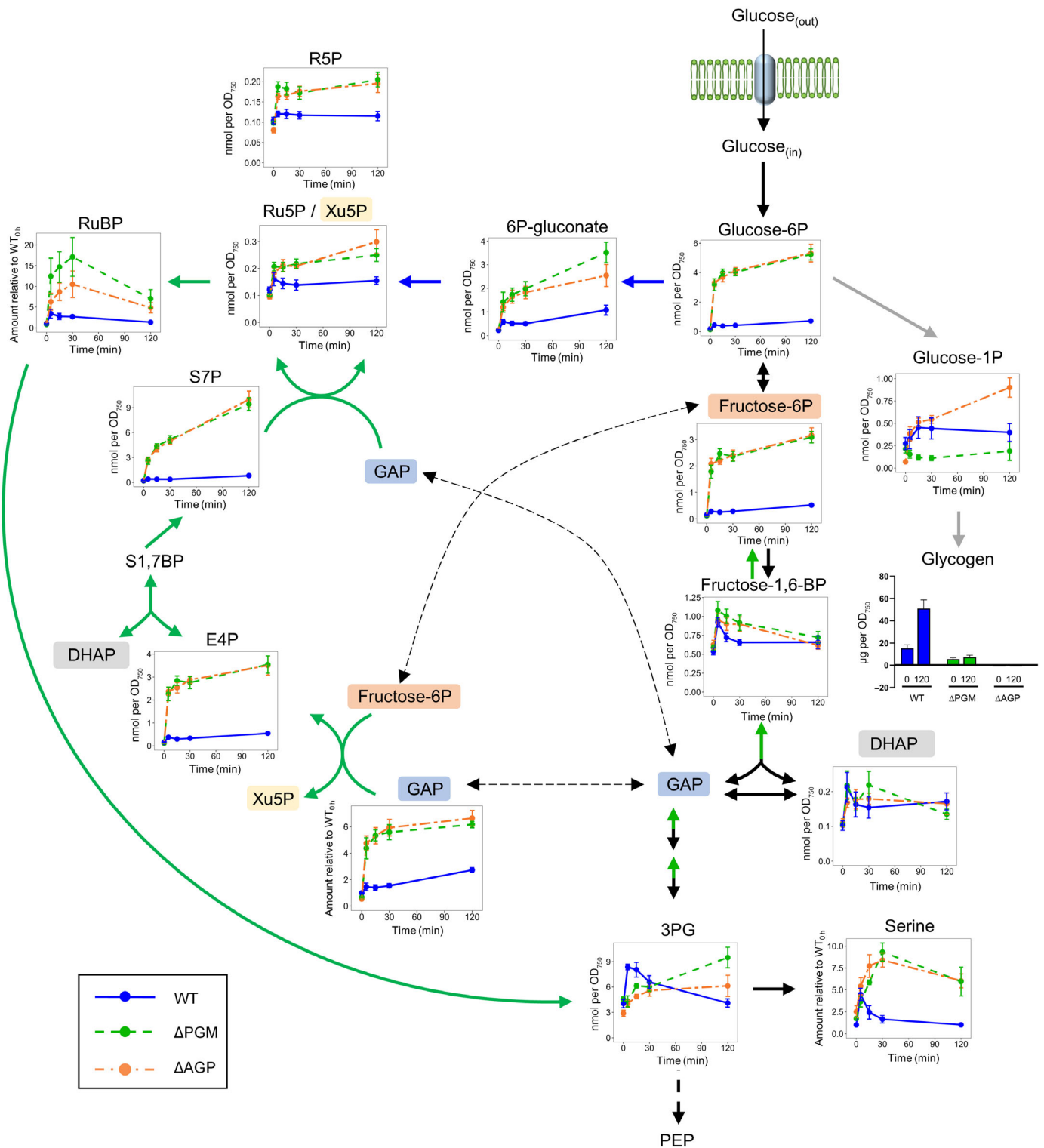


Fig. 3 Metabolic changes in upper metabolism of WT, Δ PGM and Δ AGP *Synechocystis* strains after glucose addition. Cultures of WT, Δ PGM and Δ AGP strains grown in BG11C were adjusted to a final optical density (OD_{750 nm}) of 1 and harvested before (0) and 5, 15, 30 and 120 min postglucose supplementation (2 mM). The time course displays 14 metabolites involved in glucose assimilation, the shared Oxidative Pentose Phosphate shunt (blue arrows), the Calvin-Benson-Bassham cycle (green arrows), glycogen metabolism (grey arrows) and the Entner-Meyerhof-Parnas pathway. Metabolite names highlighted with coloured rectangles refer to molecules shared with different pathways (indicated by dashed arrows). 3PG, 3P-glycerate; DHAP, dihydroxyacetone-P; E4P, erythrose-4P; GAP, glyceraldehyde-3P; R5P, ribose-5P; Ru5P/Xu5P, ribulose-5P/xylulose-5P pool; RuBP, ribulose-1,5P; S1,7BP, sedoheptulose-1,7P; S7P, sedoheptulose-7P. Values represent the mean \pm SE or fold change \pm SE relative to WT value before glucose addition of 6 independent biological replicates.

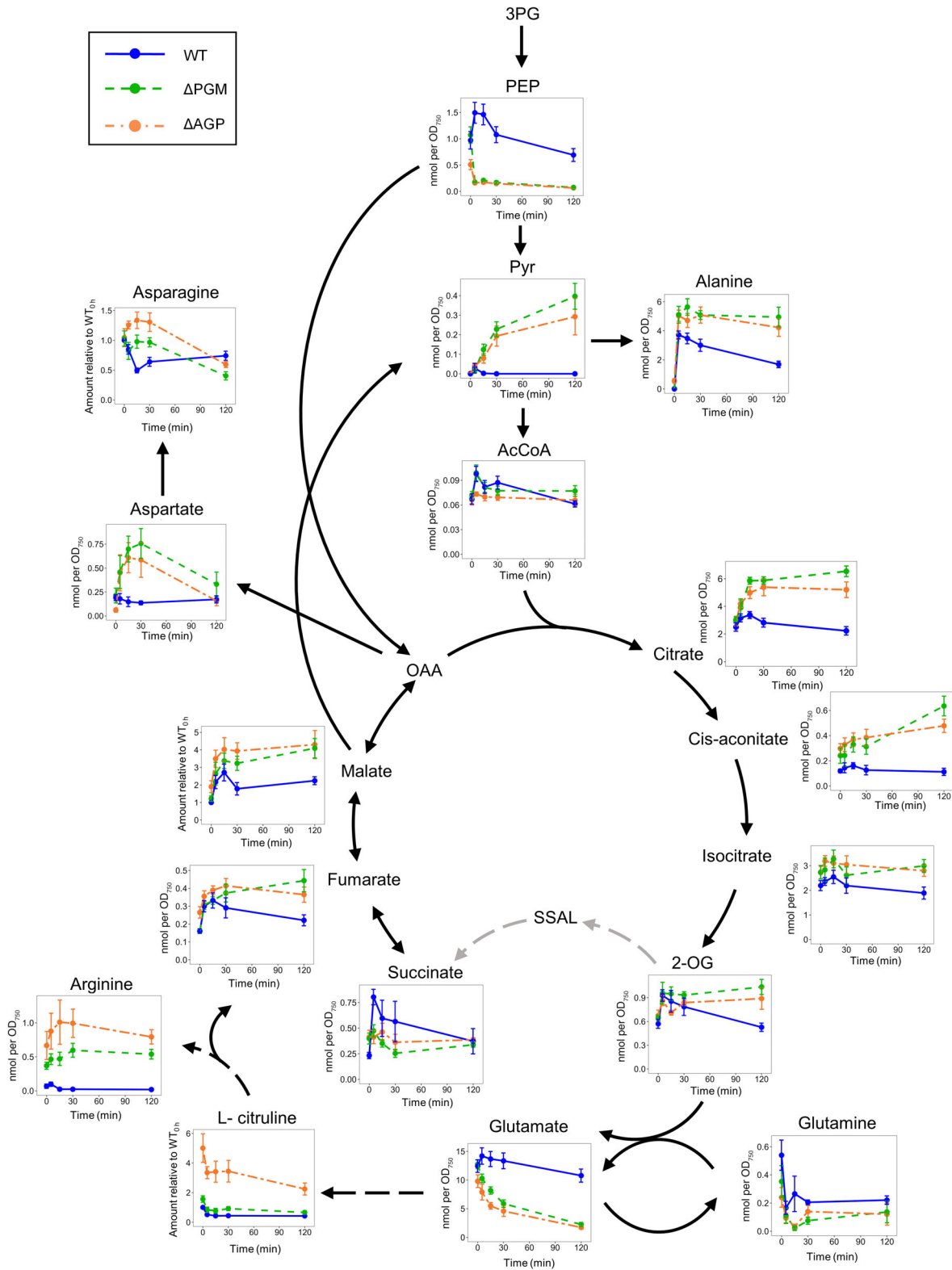


Fig. 4 Metabolic changes in 3PG downstream metabolism of WT, Δ PGM and Δ AGP *Synechocystis* strains after glucose addition. Cultures of WT, Δ PGM and Δ AGP strains grown in BG11C were adjusted to a final optical density (OD_{750 nm}) of 1 and harvested before (0) and 5, 15, 30 and 120 min postglucose supplementation (2 mM). The time course display 17 metabolites involved in lower glycolysis, tricarboxylic acid cycle and ammonium assimilation. 2-OG, 2-oxoglutarate; AcCoA, acetyl-CoA; OAA, oxalacetate; PEP, phosphoenolpyruvate; Pyr, pyruvate; SSAL, succinic semialdehyde. Dashed arrows indicate steps involving several reactions. Values represent the mean \pm SE or fold change \pm SE relative to WT value before glucose addition of 6 independent biological replicates.

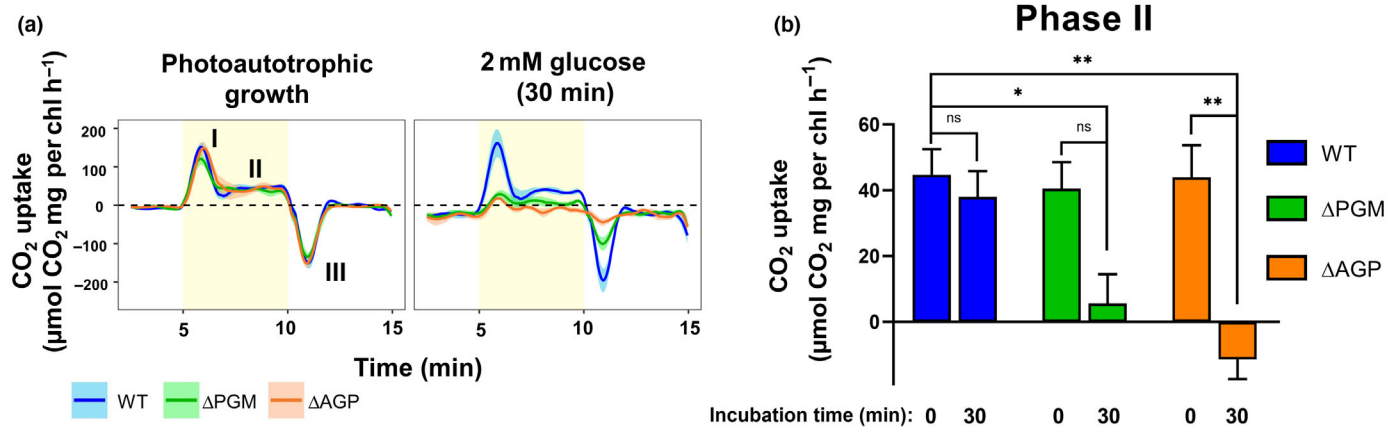


Fig. 5 Effect of glucose supplementation on the rate of CO₂ fluxes in WT, ΔPGM and ΔAGP *Synechocystis* strains determined by MIMS. (a) CO₂ exchange rates in photoautotrophy and 30 min after 2 mM glucose addition to 10 μg Chl ml⁻¹ WT, ΔPGM and ΔAGP cultures grown in BG11 measured in a Membrane Inlet Mass Spectrometer (MIMS). The yellow rectangles represent an exposure to a light intensity of 50 μmol photons m⁻² s⁻¹ while the white rectangles represent dark periods. In photoautotrophic conditions, upon the onset of light, the carbon concentration mechanism (CCM) triggered an initial concentration step absorbing high amounts of CO₂ (phase I). Subsequently, during the rest of the light period, consumption reaches a steady state (phase II). Conversely, when the lights are switched off, CCM activity ceases, leading to the release and efflux of the intracellular inorganic carbon pool back into the media (phase III). (b) Quantification of CO₂ fluxes during the steady-state in the light (phase II) in photoautotrophy or 30 min after 2 mM glucose addition. The data represent the mean ± SE from four biological replicates. Statistical significance levels are denoted by *, $P < 0.05$; **, $P < 0.01$; ns, not significant (two-way ANOVA).

We also detected photomixotrophy-induced changes in CBB cycle metabolites in the glycogen synthesis mutants. The concentrations of the ribulose-5P (Ru5P)/xylulose-5P (Xu5P) pool and ribose-5P (R5P) both doubled within 5 min of glucose addition and remained stable throughout the experiment. RuBP, however, increased > 10-fold. The metabolites S7P, E4P, and GAP exhibited similar glucose-induced patterns to G6P or F6P in the mutants, accumulating 50-, 30-, and 10-fold, respectively. By contrast, DHAP, an isomer of GAP, showed a similar trend to F1,6BP and correlated with WT values. Finally, 3PG, the product of RuBisCO, increased only transiently in WT and accumulated steadily in glycogen synthesis mutants up to twofold, which constitutes a substantial increase due to a high initial concentration. Downstream from 3PG, the first metabolite measured was PEP (Fig. 4). PEP was reduced fivefold in ΔPGM and ΔAGP 5 min after glucose addition and remained at very low levels throughout the experiment. The decrease in PEP was coupled to an increase in pyruvate, reaching > 0.25 nmol OD₇₅₀⁻¹ 120 min after glucose addition.

Levels of acetyl coenzyme A (AcCoA) remained steady in the mutants upon transition to photomixotrophy (Fig. 4). AcCoA plays a central role in cellular metabolism, serving as a key intermediate compound into the TCA cycle. Levels of most intermediates in the TCA cycle doubled, with citrate accounting for most of the carbon allocation.

Finally, amino acid pools underwent several photomixotrophy-induced changes in the glycogen synthesis mutants (Figs 3, 4, S4). Alanine and serine increased *c.* sixfold, and levels remained higher than 5 nmol OD₇₅₀⁻¹ in contrast to the transient accumulation observed in WT. Aspartate, threonine, valine and tryptophan showed transient accumulation peaking between two- and fourfold photoautotrophic levels at 30 min

after glucose addition in both glycogen synthesis mutants, compared to unchanged levels in WT. Conversely, glutamate, an amino acid essential to nitrogen assimilation in the GS-GOGAT cycle, decreased to < 2 nmol OD₇₅₀⁻¹ despite being one of the most abundant metabolites measured (> 10 nmol OD₇₅₀⁻¹ under photoautotrophic conditions). Other amino acids, such as tyrosine, phenylalanine, methionine and leucine-isoleucine were considerably depleted in ΔPGM and ΔAGP mutants, while WT showed similar levels or slight increases compared to photoautotrophy (Fig. S4b).

In summary, *Synechocystis* exhibits metabolic flexibility upon glucose addition, channelling carbon through the PGI and OPP shunts to fuel the CBB cycle, coupled with transient fluctuations in some glycolytic and TCA cycle intermediates. The impact was more pronounced in ΔPGM and ΔAGP mutants, showing rapid and sustained increases in glucose assimilation metabolites and the CBB cycle within 5 min, highlighting the crucial role of glycogen synthesis in photomixotrophic acclimation.

Photosynthesis is impaired in the glycogen synthesis mutant strains cultured with glucose

Considering the impaired growth (Fig. 2b) and decreased levels of photosynthetic proteins of the glycogen-deficient mutants under photomixotrophy (Fig. 2e), we next monitored photosynthetic performance in both photoautotrophy and 30 min post-glucose addition, capturing the metabolic overflow in both glycogen-deficient mutants (Fig. S5), but before PSII levels decreased (Fig. 2e) and before long-term acclimation to photomixotrophy.

Real-time measurement of photosynthetic CO₂ gas flux (Fig. 5) by MIMS revealed similar rates and kinetics of CO₂

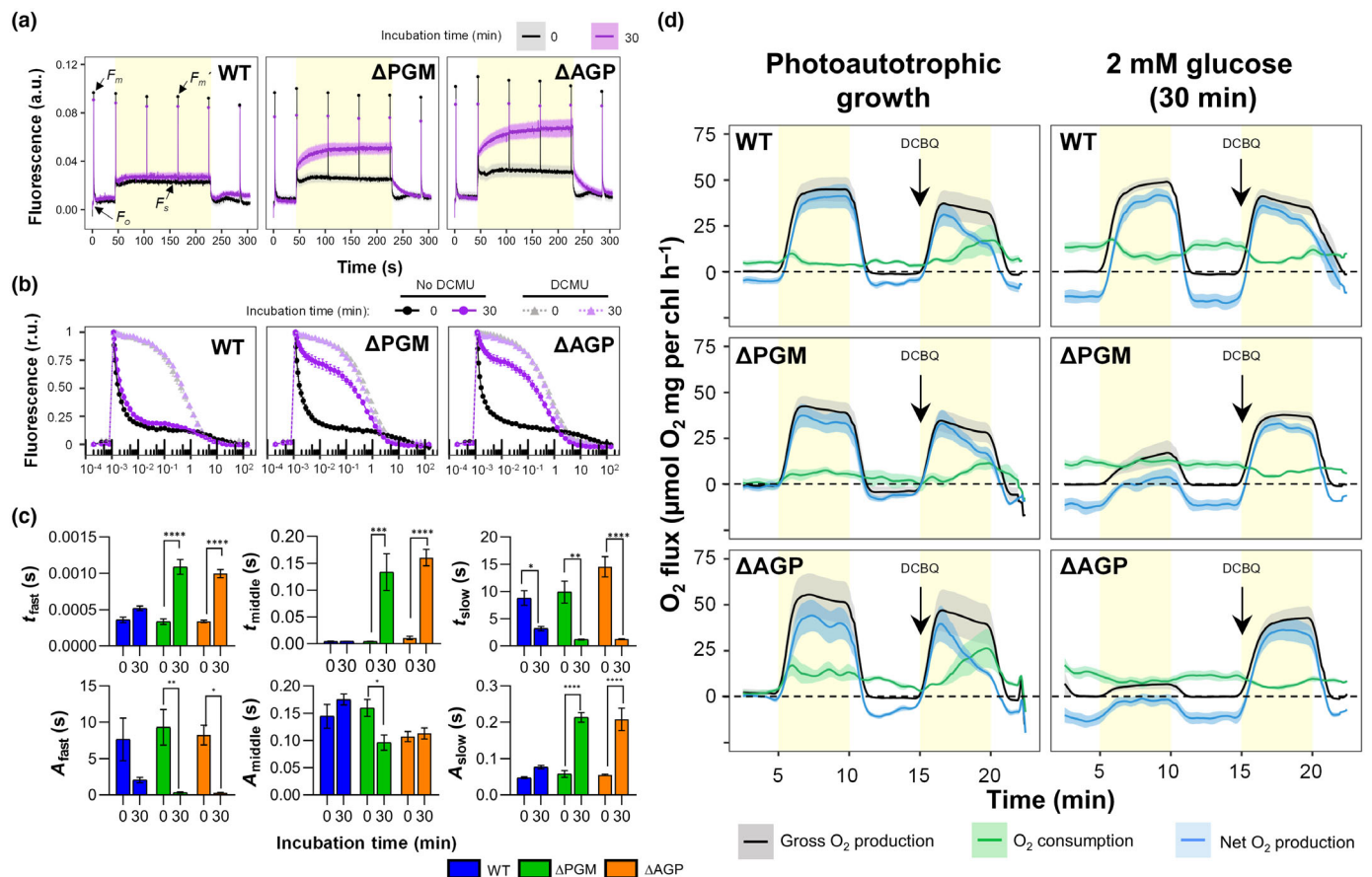


Fig. 6 Analysis of the effect of glucose supplementation on the photosynthetic and PSII performance in WT, Δ PGM, and Δ AGP *Synechocystis* strains. (a) The Chl fluorescence induction curves were generated using a DUAL-PAM-100 fluorometer using cultures of WT, Δ PGM and Δ AGP at $5 \mu\text{g Chl ml}^{-1}$ grown in BG11C in photoautotrophy (black) or 30 min after 2 mM glucose addition (purple) under $40 \mu\text{mol photons m}^{-2} \text{s}^{-1}$ actinic red light. The yellow rectangle in the background represents the light periods of the induction curve. Fluorescence parameters are indicated with black arrows: F_o represents the initial fluorescence in the dark, F_s represents the steady-state fluorescence under actinic red light, F_m represents the maximum fluorescence in the dark, F_m' represents the maximum fluorescence under the actinic light. Maximum fluorescence was determined by applying a saturation pulse (250 ms at $5000 \mu\text{mol photons m}^{-2} \text{s}^{-1}$). (b) Reoxidation kinetics of Q_A after a single-turnover saturation pulse excitation to $7.5 \mu\text{g Chl ml}^{-1}$ WT, Δ PGM and Δ AGP cultures grown in BG11 in photoautotrophy (black) or 30 min after 2 mM glucose addition (purple) using a flash fluorimeter. Fluorescence relaxation was monitored both in the absence (solid lines, circles) or in the presence (dotted line, triangle, faded colours) of $20 \mu\text{M}$ DCMU, which was added as a control to prevent Q_A^- reoxidation. (c) Analysis of the effect of glucose on the time constants (t) and the amplitudes (A) of flash-induced Chl fluorescence yield in WT, Δ PGM and Δ AGP strains. Quantification of the three phases in the reoxidation kinetics of Q_A^- by analysing the fluorescence relaxation traces from Fig. 6(b) with a three-component decay function. The initial, fast component, corresponds to the oxidation of Q_A^- by electron transfer to Q_B . The middle component corresponds to electron transfer from Q_A^- to PQ molecules from the PQ pool in the vacant Q_B^- sites. The third, slow component, derives from the recombination reactions with the oxidised S_2 state of the oxygen-evolving complex. (d) Oxygen flux dynamics in photoautotrophy and 30 min after 2 mM glucose addition using cultures of WT, Δ PGM and Δ AGP at $10 \mu\text{g Chl ml}^{-1}$ grown in BG11 in a Membrane Inlet Mass Spectrometer (MIMS). Dark periods are indicated by white rectangles, while yellow rectangles represent exposure to a light intensity of $50 \mu\text{mol photons m}^{-2} \text{s}^{-1}$. The arrows at 15 min represent the addition of 0.5 mM DCBQ. All cultures were dark-adapted for 10 min before the measurements. The data represent the mean \pm SE from four (a and d) and five (b and c) biological replicates. Statistical significance levels are denoted by *, $P < 0.05$; **, $P < 0.01$; ***, $P < 0.001$; ****, $P < 0.0001$; otherwise, not significant (two-way ANOVA).

uptake during photoautotrophy in all strains. While WT maintained photoautotrophic CO_2 uptake kinetics in the presence of glucose (Fig. 5a), Δ PGM and Δ AGP mutants showed negligible steady-state CO_2 uptake rates (Fig. 5b). Additionally, the glycogen synthesis mutants exhibited diminished maxima and minima of CO_2 uptake rates during dark-to-light (phase I, Fig. S6) and light-to-dark (phase III, Fig. S6) transitions, respectively, associated with the import of CO_2 by the light-activated carbon concentration mechanism (CCM) and export of CO_2 .

The decrease in carbon uptake (Fig. 5) occurred already before ROS accumulation (Fig. 2), or as indicated by both immunoblotting (Fig. 2) and 77K fluorescence emission spectra (Fig. S7; Methods S2), before any change in the PSII/PSI ratio. This prompted us to investigate potential disturbance of photosynthetic electron transport. First, we conducted a saturating pulse analysis of Chl fluorescence. In photoautotrophic conditions, the Chl fluorescence traces (Fig. 6a) and PSII effective yields [$Y(\text{II})$] were similar (Fig. S8). After 30 min incubation with glucose, the

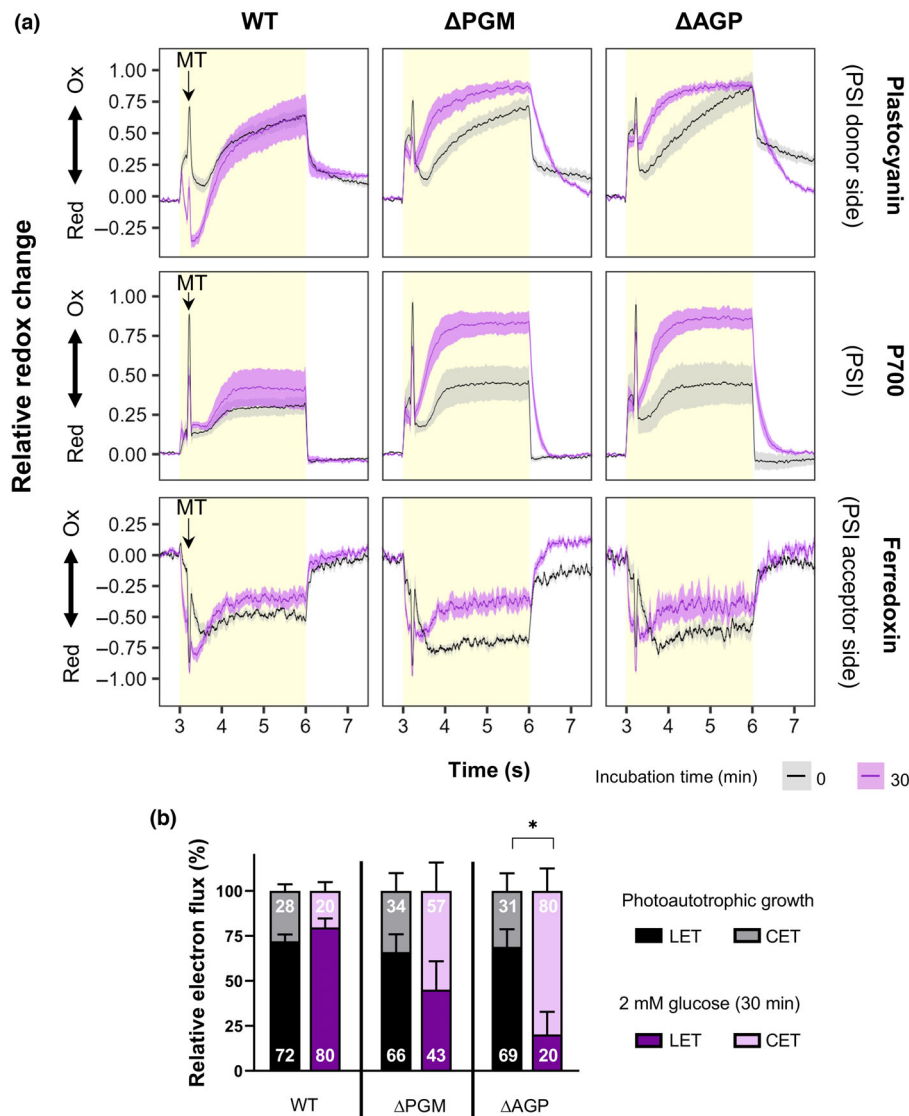


Fig. 7 PSI redox characterisation and electron flow in the PETC in photoautotrophy and 30 min after glucose addition in *Synechocystis*. (a) Analysis of the redox state changes of P700 (PSI), Plastocyanin (PC) and Ferredoxin (Fd). Maximum amplitudes of these components were determined by (near-infrared) NIR absorption using a NIRMAL script implemented in a DUAL-KLAS-NIR instrument. WT, Δ PGM and Δ AGP strains were cultured in BG11 in photoautotrophy or supplemented with 2 mM glucose for 30 min. The cultures were adjusted to a concentration of 20 $\mu\text{g Chl ml}^{-1}$. PC, P700 and Fd redox changes were deconvoluted from the initial absorbance differences (780–820, 820–870, 840–965 and 870–965 nm). Differential model plots (model spectra) that were specifically determined for *Synechocystis* were used in the deconvolution process. Multiple turnover flashes (MT, indicated by the arrow) were provided following the light onset to fully reduce Fd. The traces were normalised using the maximal levels of Fd reduction and P700 oxidation observed in each sample. Dark periods are indicated by white rectangles, while yellow rectangles represent exposure to light intensity of 200 $\mu\text{mol photons m}^{-2} \text{s}^{-1}$. (b) Contribution of the linear and cyclic electron transport pathways to total PSI electron flux in intact WT, Δ PGM and Δ AGP cells grown in BG11 determined using a DUAL-KLAS-NIR system. The data represent the mean \pm SE from nine (a) and five (b) biological replicates. Statistical significance levels are denoted in (b) by *, $P < 0.05$ (two-way ANOVA).

WT strain showed unchanged fluorescence kinetics (Fig. 6a) and a slightly, albeit not significantly, lower Y(II) (Fig. S8). By contrast, the glycogen synthesis mutants exhibited higher F_s levels, resulting in an approximate halving of Y(II) (Fig. S8).

The increase in flash-induced Chl fluorescence and its subsequent relaxation in darkness derive from the reduction and reoxidation of Q_A^- , respectively, reflecting the status of the acceptor side of the PSII complex (Vass *et al.*, 1999). When the fluorescence curves are fitted with a three-component decay function, the initial, fast component corresponds to oxidation of Q_A^- by electron transfer to Q_B , the middle component corresponds to electron transfer from Q_A^- to PQ molecules binding to empty Q_B sites, while the third, slow component derives from recombination reactions, mainly with the S_2 state of the oxygen-evolving complex (Vass *et al.*, 1999). In the presence of glucose, WT exhibited only slightly, and nonsignificantly slower relaxation of flash-induced fluorescence, in comparison to photoautotrophic cultures. By contrast, in both mutants reoxidation of Q_A^- was slowed down significantly 30 min after treatment with glucose

(Fig. 6b). The time constant for the fluorescence decay in the fast phase increased from *c.* 0.35 ms to 1 ms in both glycogen synthesis mutants, while the time constants for the middle phase increased exponentially from *c.* 4 and 10 ms to 133 and 161 ms for the Δ PGM and Δ AGP mutants, respectively (Fig. 6c). The amplitude of the fast component was *c.* six- to sevenfold lower and the amplitude of the slow component was *c.* threefold higher in the glycogen synthesis mutants in comparison to WT 30 min after introduction of glucose (Fig. 6c). The amplitude of the middle component, however, was only slightly affected. These results suggest that electron transfer from Q_A^- to Q_B is inhibited and recombination reactions are increased in a large sub-population of PSII centres in the glycogen synthesis mutants. The kinetics of Q_A^- reoxidation of photomixotrophic glycogen synthesis mutants were intermediate between photoautotrophic and samples treated with DCMU, an inhibitor that occupies the Q_B site in PSII and prevents Q_A^- oxidation (Fig. 1). In the presence of DCMU, Q_A^- reoxidation occurs via charge recombination with donor side components. Therefore, we concluded that glucose

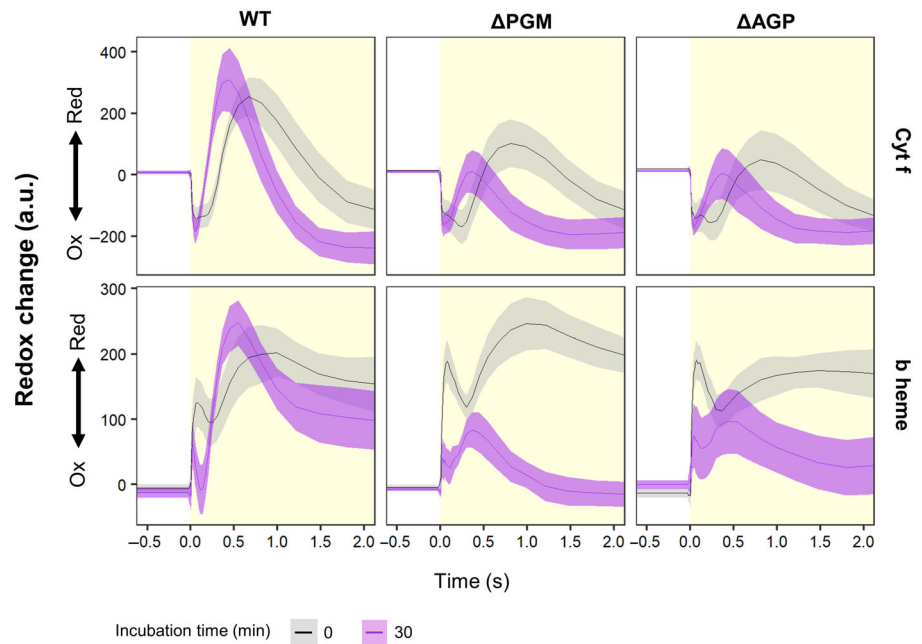


Fig. 8 Redox state changes of cytochrome b_6f components in photoautotrophy and 30 min after glucose addition in *Synechocystis*. Analysis of the redox state change of cytochrome f (Cyt f) and b heme from cytochrome b_6f in a JTS-10 spectrophotometer and its software. WT, Δ PGM and Δ AGP strains were cultured in photoautotrophy or supplemented with 2 mM glucose for 30 min. The cultures were adjusted to a concentration of $7.5 \mu\text{g Chl ml}^{-1}$. The light periods are represented by the yellow rectangle in the background. The data represent the mean \pm SE from five biological replicates.

induces substantial changes on the acceptor side of PSII in the glycogen synthesis mutants, whereas the PSII donor side remains unaffected.

Subsequently, we employed MIMS to investigate how these alterations in electron transfer affect the photosynthetic oxygen fluxes (Figs 6d, S8). In photoautotrophy, all strains displayed similar fluxes, apart from slightly higher light-induced O_2 uptake in the Δ AGP mutant. In the presence of glucose respiration was expectedly increased in all strains (Fig. S9, O_2 uptake). More strikingly, both glycogen synthesis mutants exhibited a drastic decrease in photosynthetic gross and net O_2 production, with the Δ AGP strain being more severely affected (Fig. S9). Intriguingly, addition of glucose to photoautotrophically grown Δ AGP cultures caused an immediate decline in O_2 evolution (Fig. S10). The addition of sorbitol had no effect (Fig. S10), indicating osmotic interference was not at play.

Based on the flash fluorescence results (Fig. 6b), we hypothesised that the decrease in O_2 evolution in photomixotrophic glycogen synthesis mutants was due to inhibition of electron transfer from PSII. Accordingly, addition of 2,6-dichloro-1,4-benzoquinone (DCBQ), an artificial electron acceptor that acts before Q_B (Fig. 1), restored the light-induced oxygen evolution rates in the mutants to levels comparable to those in photoautotrophic conditions (Figs 6d, S9). These results are in line with the Q_A^- relaxation experiments (Fig. 6b), confirming a blockage on the acceptor side of PSII, while the PSII donor side including the oxygen-evolving complex is functional, as artificially oxidising Q_A^- by DCBQ alleviates the blockage.

To assess the impact of partial inhibition of electron transfer at PSII on downstream reactions, we measured the redox changes in PSI reaction centre Chl P700, the electron donor to PSI, PC, and the electron acceptor from PSI, Fd. Consistent with inhibited electron transfer from PSII, both PC and P700 became strongly oxidised to *c.* 75% of their maximal oxidation levels within *c.* 1 s

of illumination in the glycogen synthesis mutants in the presence of glucose (Fig. 7a). However, they exhibited similar redox kinetics in far-red light, preferentially exciting PSI, as photoautotrophic cultures (Fig. S11). Therefore, the partial inhibition of electron transfer at PSII in the presence of glucose had downstream effects on redox changes in PSI and associated electron carriers, but PSI was functional. By contrast, after addition of glucose, the WT strain showed strong, transient reduction of PC below the dark level and only moderately increased oxidation of P700 to *c.* 40% of the maximum level by 1.5 s of illumination (Fig. 7a). Interestingly, oxidation of P700 and concomitant reduction of Fd were inhibited in WT cells under far-red light after the addition of glucose (Fig. S11). This suggests that PSI to Fd electron transfer is limited, suggesting control at the acceptor side of PSI in photomixotrophy.

Estimation of the relative contributions of CET and the LET to the total electron transport rate through PSI (Theune *et al.*, 2021) showed that all the strains have similar fluxes under photoautotrophic conditions, with LET contributing almost 70% of the total flux (Fig. 7b). However, this value might be lower since the method's limitation due to the employment of DCMU could underestimate CET quantification (Theune *et al.*, 2021). 30 min after glucose addition, however, both glycogen synthesis mutants, but Δ AGP in particular, displayed an increase in CET contribution due to LET reductions, while WT retained the same ratio.

To further dissect the cause of the inhibition of electron transport from PSII, we analysed the redox kinetics of the b hemes and Cyt f of the Cyt b_6f complex (Fig. 8). Under photoautotrophy, all strains displayed similar b heme redox kinetics. However, while the redox kinetics of Cyt f and the magnitude of light-induced oxidation were similar between all strains, the maximal reduction of Cyt f in the glycogen synthesis mutants was approximately half of WT levels.

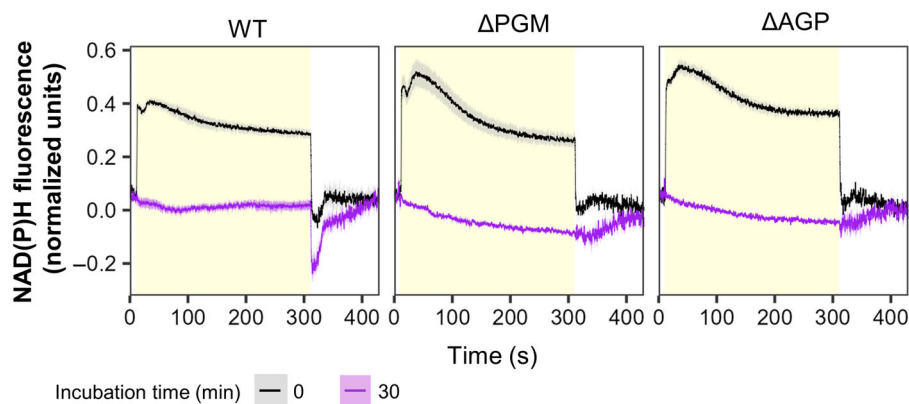


Fig. 9 NAD(P)H fluorescence in photoautotrophy and 30 min after glucose addition in WT, Δ PGM and Δ AGP *Synechocystis* strains. NAD(P)H fluorescence light-dependent kinetics of WT, Δ PGM and Δ AGP cultures at $7.5 \mu\text{g Chl ml}^{-1}$ grown in BG11 in photoautotrophy (black) or 30 min after 2 mM glucose addition (purple) measured in a DUAL-PAM-100 fluorometer. The light periods are represented by the yellow rectangle in the background. Traces were normalised by subtracting the minimum value of the preilluminated fluorescence. The data represent the mean \pm SE from four biological replicates.

Addition of glucose increased the transient oxidation of the *b* hemes in WT to dark-adapted levels and sped up their re-reduction while resulting in a strong decrease in the maximal reduction of the *b* hemes in both glycogen synthesis mutants. The light-induced re-reduction kinetics of Cyt *f* were shifted earlier in all strains upon the addition of glucose, suggesting possible alteration in *Q* cycle operation in response to the increased level of respiration (Fig. 6d). The re-reduction of Cyt *f* increased slightly in glucose-treated WT but importantly, not in the glycogen synthesis mutants. In DCMU-treated WT cells the re-reduction of Cyt *f* is decreased *c.* fourfold from photoautotrophic levels (Solymosi *et al.*, 2020), so here the glucose-treated glycogen synthesis mutants displayed intermediate Cyt *f* kinetics between photoautotrophic and DCMU-treated samples (similar to Q_A^- reoxidation kinetics, Fig. 6b). These results reflect a donor side limitation of PSI in the glycogen synthesis mutants in the presence of glucose and indicate that it is unlikely that an overreduced PQ pool would be the cause for the limitation of electron transport from PSII.

As altered redox kinetics of photosynthetic electron transport in the presence of glucose are likely to affect the NAD(P)⁺/NAD(P)H pools, we next explored the light-induced NAD(P)⁺/NAD(P)H redox dynamics by monitoring NAD(P)H fluorescence. Under photoautotrophic conditions, dark-adapted cultures showed a rapid rise in fluorescence upon illumination, indicating the photosynthetic reduction of NADP⁺ by ferredoxin-NADP⁺ reductase (FNR). After the illumination period, the fluorescence signal decayed due to continued NADPH consumption in the CBB cycle. Subsequent dark-induced inactivation of the CBB cycle and activation of the OPP pathway then led to a resurgence in fluorescence, reaching levels similar to those in dark-adapted cells (Fig. 9).

In the presence of glucose, none of the strains exhibited light-induced increase in NAD(P)H fluorescence, indicating strong reduction of NADP⁺ already in the dark via the OPP shunt (Ogawa *et al.*, 2021). In contrast to the Δ PGM and Δ AGP mutants, the WT strain actively used NAD(P)H pools as evidenced by the fast decay of the signal upon the light–dark transition, followed by a subsequent recovery of NAD(P)H fluorescence close to dark-adapted levels.

Discussion

Transcriptomic analyses from photoautotrophy to photomixotrophy show only minor differences in carbon metabolism-related gene expression (Kahlon *et al.*, 2006; Lee *et al.*, 2007; Haimovich-Dayana *et al.*, 2011; Yoshikawa *et al.*, 2013), suggesting that adjustment to photomixotrophy is mainly mediated by an unchanged pre-existing set of enzymes (Muth-Pawlak *et al.*, 2022). In this work, we show that glycogen synthesis is crucial for acclimation to photomixotrophy. Its impairment induces rapid and profound metabolic alterations in *Synechocystis*, accompanied by inhibition of photosynthetic electron transport from PSII, and ultimately results in cell death.

The addition of glucose enhances growth and glycogen reserves increase (Fig. 2b,c) but eventually, over several days, reduces the photosynthetic capacity (Solymosi *et al.*, 2020). Similarly, starch accumulation and subsequent limitations in photosynthetic capacity were observed in the monocot *Spirodela polyrhiza* 7498 after glucose addition (Sun *et al.*, 2023). During this acclimation, glycogen becomes essential since impairments in the glycogen synthesis pathway, such as those in the Δ PGM and Δ AGP mutants, result in reduced fitness in the presence of glucose (Figs 2–4, 6, 7, S3, Gründel *et al.*, 2012). These findings are consistent with other conditions where glycogen accumulates, such as high light or nitrogen deprivation, when the inability to accumulate glycogen impedes acclimation and leads to growth arrest or even cell death (Cano *et al.*, 2018; Doello *et al.*, 2022; Ortega-Martínez *et al.*, 2023).

In this context, metabolic profiling highlighted several important findings. Under photoautotrophic conditions, WT and both the Δ PGM and Δ AGP mutants display similar metabolic profiles (Figs 3, 4, S4; Table 1). Under these conditions, impaired glycogen metabolism does not alter the carbon management of cells (Cano *et al.*, 2018) nor affect photosynthetic parameters (Figs 6, 7, 9). Upon glucose supplementation, WT rapidly incorporates glucose into metabolism, leading to transient alterations in the metabolic landscape (Figs 3, 4) and rapid glycogen accumulation (Fig. 2c). This suggests that cyanobacteria directly store a major portion of G6P as glycogen, consistent with previous findings (Yoshikawa *et al.*, 2013; Nakajima *et al.*, 2014; Schulze *et al.*, 2022). Thus, 120 min after glucose addition, the sum of

Table 1 Abundance of metabolites^a from the first steps in glucose assimilation (phosphoglucose isomerase and oxidative pentose phosphate shunts and phosphoglucomutase), Calvin–Benson–Bassham cycle and lower glycolysis in WT, ΔPGM and ΔAGP *Synechocystis* strains.

	Incubation time (min)	WT	ΔPGM	ΔAGP
Metabolites ^a (nmol OD ₇₅₀ ⁻¹)	0	2.67 ± 0.17	2.72 ± 0.07	2.67 ± 0.27
	30	7.00 ± 0.63	23.54 ± 1.63	23.37 ± 1.29
	120	7.05 ± 0.73	31.93 ± 2.69	30.73 ± 3.15

^aMetabolites: summation of glucose-1P, glucose-6P, 6-phosphogluconate, fructose-6P, fructose-1,6-BP, ribulose-5P/Xilulose-5P, ribose-5P, erythrose-4P, sedoheptulose-7P, dihydroxyacetone phosphate, glyceraldehyde phosphate, phosphoenolpyruvate, pyruvate and alanine. Data represent the mean ± SE of six biological replicates.

the concentrations of the main metabolites in the OPP and PGI shunts and the CBB cycle (including gluconeogenic EMP) increased 2.63-fold (Table 1). By contrast, when glycogen synthesis is limited, metabolites from those pathways accumulate to > 11-fold their initial levels in both mutant strains while growth was impeded and there was little glucose consumption (Fig. 2b, d). This parallel behaviour is noteworthy, given the differences in glycogen accumulation although glycogen reserves were hardly increased in the ΔPGM strain upon introduction of glucose (Fig. 2c). Therefore, the limited phosphoglucomutase activity of the ΔPGM mutant forces redirection of G6P into central metabolism, overcoming the potential buffer effect of glycogen storage and ultimately behaving like ΔAGP, a completely glycogen-less strain.

Finally, the consistent increase in 6PG observed in all strains suggests a stoichiometrically equal NADPH synthesis from the OPP shunt (Figs 1, 3), as both 6PG and NADPH are products of G6PDH. This likely resulted in near complete reduction of the NADP⁺/NADPH ratio even in darkness, which is consistent with NAD(P)H fluorescence kinetics. There was no further increase in fluorescence upon dark-to-light transitions, and the photosynthetic consumption of NADPH in light by the CBB cycle was roughly equal to the rate of light-induced NADP⁺ reduction (Fig. 9). When glycogen cannot be synthesised, another intermediate accumulated is pyruvate. Electrons could be diverted from pyruvate to Fd via the pyruvate-ferredoxin oxidoreductase (PFOR) (Wang *et al.*, 2022). Reduced Fd is the electron donor to the NDH-1 complex (Schuller *et al.*, 2019), which then injects electrons to the PQ pool. Therefore, glycogen synthesis prevents the overreduction of the electron transport chain in the presence of glucose. In the glycogen synthesis mutants, overreduction of the PETC is prevented by prompt inhibition of electron transfer from PSII.

Addition of glucose diminished CO₂ uptake and O₂ evolution in the ΔPGM and ΔAGP mutants (Figs 5, 6d, S6). A similar effect was observed in *Chlamydomonas*, where photosynthetic capacity was slightly reduced when cells were grown in photomixotrophy using acetate as the source of organic carbon (Heifetz *et al.*, 2000; Roach *et al.*, 2013). Similarly, *Synechocystis* strains genetically engineered to incorporate exogenous acetate showed reduced O₂ evolution (Thiel *et al.*, 2017), and prolonged subjection of *Synechocystis* WT to glucose for several days also results in closure of PSII reaction centres and diminished O₂ evolution (Solymosi *et al.*, 2020). Although we cannot fully exclude the

inhibition of PSII activity in the mutants in the presence of glucose being due to strong reduction of the PQ pool, the decreased light-induced reduction of the *b* hemes and Cyt *f* of the Cyt *b₆f* complex suggests that is unlikely, as there are less electrons fed to the *Q* cycle from the PQ pool (Fig. 8). Light-induced reduction of Cyt *f* is not fully inhibited in the glycogen synthesis mutants though, as it is in WT after 3 d of photomixotrophy or in the presence of DCMU (Solymosi *et al.*, 2020). This suggests that the mechanism of PSII inhibition induced by long-term photomixotrophy may differ from the rapid inhibition observed in the glycogen synthesis mutants. In these mutants, the effects on photosynthetic activity are likely caused by an inhibitory effect on Q_A⁻ to Q_B electron transfer at PSII. This could result from replacement of the bicarbonate associated with the nonheme iron by small metabolites such as acetate, formate, glycolate or lactate (Fig. 10; Wydrzynski & Govindjee, 1975; Berthomieu & Hiernerwadel, 2001; Ishikita *et al.*, 2007; Shevela *et al.*, 2007). The impairment of electron transfer due to bicarbonate displacement would affect the midpoint potential of the Q_A/Q_A⁻ couple (Brinkert *et al.*, 2016) and, therefore, its redox dynamics. We observed this effect in the single flash fluorescence experiments, where slow Q_A⁻ reoxidation was observed in the glycogen synthesis mutants in the presence of glucose (Fig. 6b) when metabolic changes were already evident (Fig. S5; Table 1). The diminished amplitudes of the fast component of Chl fluorescence decay and increased amplitudes of the slow component further supported impaired Q_A⁻ to Q_B electron transfer and increased ROS-inducing recombination reactions within PSII, respectively, in the mutants in the presence of glucose (Fig. 6c). The hypothesis of inhibition of electron transfer from Q_A⁻ is also supported by diminished O₂ evolution being rescued by the addition of the artificial electron acceptor DCBQ (Figs 6d, S9, S10). DCBQ can take electrons from Q_A⁻, and, as reported recently, likely also directly from the peripheral Chls in PSII (Baikie *et al.*, 2023). Restoration of O₂ evolution by DCBQ addition has also been observed in photomixotrophic *Chlamydomonas* (Roach *et al.*, 2013). A similar effect on Q_A redox state could also be observed under nitrogen depletion, where photosynthesis is minimal (Ogawa & Sonoike, 2016). The cytochrome *c_M* (CytM) protein is necessary for photomixotrophy-induced closure of PSII (Solymosi *et al.*, 2020). CytM has been suggested to function in the reduction of nitric oxide (NO) (Rodríguez-Gil *et al.*, 2021) which, interestingly, also inhibits electron transfer from PSII (Solymosi *et al.*, 2022). However, the molecular mechanism of CytM, and

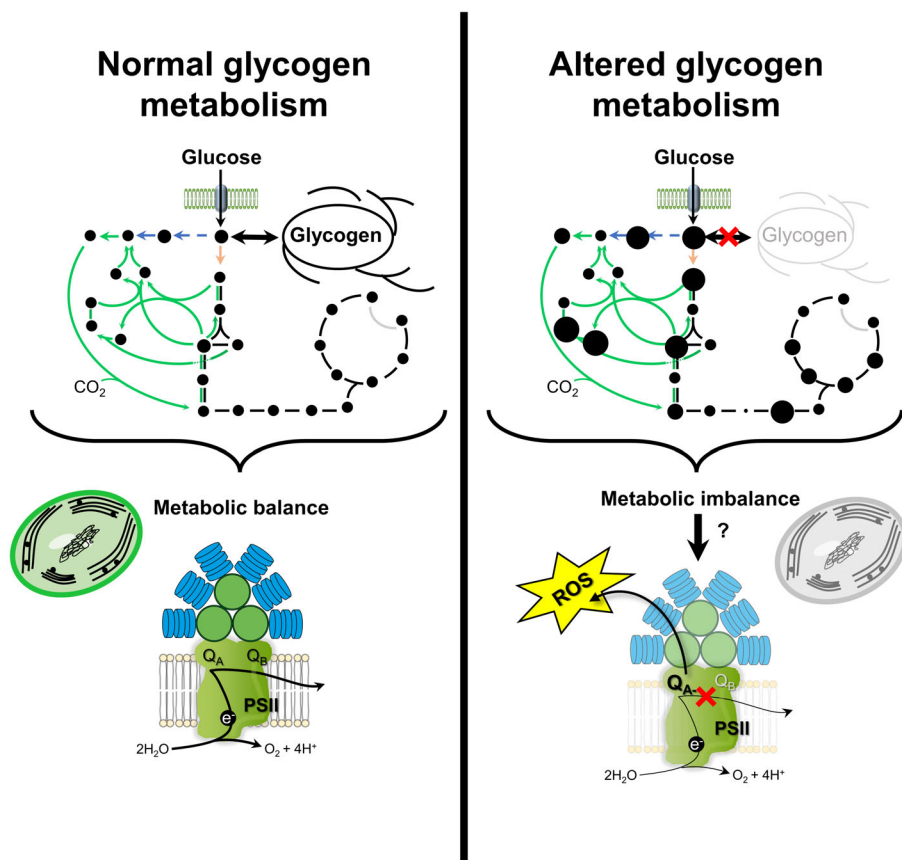


Fig. 10 The role of glycogen in the metabolic adaptation to photomixotrophy and its interconnection with photosynthesis in *Synechocystis*. The uptake of glucose for cellular metabolism in photoheterotrophically growing cells induces changes in the metabolic profile, with part of the carbon relocated as glycogen. This allows for a smooth transition to photomixotrophic conditions. However, impaired glycogen metabolism forces the redirection of glucose uptake to central carbon metabolism, causing a metabolic overflow within minutes. This imbalance affects the electron transfer at the donor side of PSII. Plausible causes of photosynthesis blockage include bicarbonate displacement within PSII by metabolic analogues or induction of secondary regulatory mechanisms mediated by proteins associated with PSII. This blockage eventually leads to an increase in reactive oxygen species production, hindering viability. Metabolites are depicted as dots with a size representing its concentration and are connected by lines (blue for OPP shunt, green for CBB cycle, orange for PGI shunt and the rest in black).

whether the phenotypes of the glycogen synthesis mutants are connected to CytM or NO signalling remains to be elucidated.

Another explanation could involve small PSII-binding proteins. For example, the absence of cyanobacterial PsbJ extends the lifetime of Q_A^- , stalling electron flow to Q_B and limiting O_2 evolution (Shi *et al.*, 2012). PsbQ' from the red alga *Cyanidium caldarium* modulates the reduction potential of Q_A making the formation of triplet Chls less likely, thereby providing photoprotection (Yamada *et al.*, 2018). In *Nicotiana tabacum* L, PSII inactivation caused by PsbS/Psb27 was relieved by bicarbonate addition, restoring normal Q_A reoxidation (Fantuzzi *et al.*, 2023). The promptness of the glucose-induced alterations of photosynthetic performance suggests that the adjustments in PSII are probably post-translational and induced by the metabolic changes.

The inhibition of Q_A^- to Q_B electron transfer could lead to photodamage by ROS formation via charge recombination in PSII (Figs 2f, 10) (Fufezan *et al.*, 2007). This would affect the lifecycle of PSII proteins, especially of D1, a core subunit of the reaction centre with a fast turnover (Latifi *et al.*, 2009). Loss of D1 is characteristic of various stress conditions (Murata *et al.*, 2007; Johnson & Pakrasi, 2022), and we also observed loss of D1 in the photomixotrophic glycogen synthesis mutants (Fig. 2e). The PSII damage likely exceeded the turnover capacity of its repair cycle, leading to more ROS production and ultimately, unless glucose is removed, cell death (Figs 2a,b, S3). As both the photosynthetic and respiratory electron transport

reactions occur on the thylakoid membranes in cyanobacteria, partly sharing components, the transition to photomixotrophic conditions requires coordination of the bioenergetic and metabolic pathways of the cell. Understanding this coordination is vital for optimising biotechnological applications exploiting photosynthesis in the presence of an organic carbon source, yet these processes have remained poorly characterised (Wan *et al.*, 2015; Kanno *et al.*, 2017). In the current study, we revealed that the glycogen metabolism plays a pivotal role in the crosstalk between the metabolic state of the cell and the bioenergetic pathways of photosynthesis and respiration, allowing maintenance of source/sink balance in the cyanobacterial cell, and enabling growth in diverse trophic modes. While further research on the signalling pathways and molecular mechanisms involved is needed, our study provides foundations for re-engineering cyanobacterial bioenergetics and carbon metabolism for optimised, sustainable production of desired compounds under photomixotrophic conditions.

Acknowledgements

This work was funded by grants PID2019-104513GB-I00 and PID2022-138317NB-I00 both financed by MCIU/AEI/10.13039/501100011033/FEDER Una manera de hacer Europa' and by Junta de Andalucía, Group BIO-0284 to FJF and financially supported by the NordForsk Nordic Center of Excellence 'NordAqua' (no. 82845 to YA), the Novo Nordisk

Foundation project 'PhotoCat' project (no. NNF20OC0064371 to YA). PO-M is a recipient of grant FPU18/06580 from the Ministerio de Universidades and an EMBO Scientific Exchange Grant. We thank Dr Tuomas Huokko and Michal Hubacek for assistance with PO-M's research visit to University of Turku, and Dr Luis López-Maury for critical reading of the manuscript. The photosynthetic electron transport studies (except Chl fluorescence analysis) were conducted in the PhotoSYN Finnish Infrastructure for Photosynthesis Research.

Competing interests

None declared.

Author contributions

SD-T and FJF conceived the research, all the authors designed the research, PO-M: performed all the experiments, and wrote the manuscript draft; LN performed MIMS measurements and drafted the photosynthesis section; SD-T supervised physiological and metabolomics experiments; LTW developed photosynthesis experiment analysis scripts; FJF and YA, funding acquisition; all the authors revised and approved the manuscript. PO-M and LN contributed equally to this work.

ORCID

Yagut Allahverdiyeva  <https://orcid.org/0000-0002-9262-1757>

Sandra Díaz-Troya  <https://orcid.org/0000-0002-5878-9062>

Francisco J. Florencio  <https://orcid.org/0000-0002-2068-7861>

Lauri Nikkanen  <https://orcid.org/0000-0002-7192-9322>

Pablo Ortega-Martínez  <https://orcid.org/0000-0001-5508-5636>

Laura T. Wey  <https://orcid.org/0000-0003-2345-0699>

Data availability

The data that support the findings of this study are available in the article and its [Supporting Information](#).

References

- Baikie TK, Wey LT, Lawrence JM, Medipally H, Reisner E, Nowaczyk MM, Friend RH, Howe CJ, Schnedermann C, Rao A *et al.* 2023. Photosynthesis rewired on the pico-second timescale. *Nature* 615: 836–840.
- Ball SG, Morell MK. 2003. From bacterial glycogen to starch: understanding the biogenesis of the plant starch granule. *Annual Review of Plant Biology* 54: 207–233.
- Beckmann K, Messinger J, Badger MR, Wydrzynski T, Hillier W. 2009. On-line mass spectrometry: membrane inlet sampling. *Photosynthesis Research* 102: 511–522.
- Berthomieu C, Hienerwadel R. 2001. Iron coordination in photosystem II: interaction between bicarbonate and the Q_B pocket studied by Fourier transform infrared spectroscopy. *Biochemistry* 40: 4044–4052.
- Brinkert K, De Causmaecker S, Krieger-Liszky A, Fantuzzi A, Rutherford AW. 2016. Bicarbonate-induced redox tuning in Photosystem II for regulation and protection. *Proceedings of the National Academy of Sciences, USA* 113: 12144–12149.
- Burnap RL, Hagemann M, Kaplan A. 2015. Regulation of CO₂ concentrating mechanism in cyanobacteria. *Life* 5: 348–371.
- Cano M, Holland SC, Artier J, Burnap RL, Ghirardi M, Morgan JA, Yu J. 2018. Glycogen synthesis and metabolite overflow contribute to energy balancing in cyanobacteria. *Cell Reports* 23: 667–672.
- Carrieri D, Paddock T, Maness PC, Seibert M, Yu J. 2012. Photo-catalytic conversion of carbon dioxide to organic acids by a recombinant cyanobacterium incapable of glycogen storage. *Energy and Environmental Science* 5: 9457–9461.
- Cifuentes JO, Comino N, Trastoy B, D'Angelo C, Guerin ME. 2019. Structural basis of glycogen metabolism in bacteria. *Biochemical Journal* 476: 2059–2092.
- Díaz-Troya S, López-Maury L, Sánchez-Riego AM, Roldán M, Florencio FJ. 2014. Redox regulation of glycogen biosynthesis in the cyanobacterium *Synechocystis* sp. PCC 6803: analysis of the AGP and glycogen synthases. *Molecular Plant* 7: 87–100.
- Doello S, Neumann N, Forchhammer K. 2022. Regulatory phosphorylation event of phosphoglucomutase 1 tunes its activity to regulate glycogen metabolism. *FEBS Journal* 289: 6005–6020.
- Fantuzzi A, Haniewicz P, Farci D, Loi MC, Park K, Büchel C, Bochtler M, Rutherford AW, Piano D. 2023. Bicarbonate activation of the monomeric photosystem II-PsbS/Psb27 complex. *Plant Physiology* 192: 2656–2671.
- Field CB, Behrenfeld MJ, Randerson JT, Falkowski P. 1998. Primary production of the biosphere: integrating terrestrial and oceanic components. *Science* 281: 237–240.
- Fufezan C, Gross CM, Sjödin M, Rutherford AW, Krieger-Liszky A, Kirilovsky D. 2007. Influence of the redox potential of the primary quinone electron acceptor on photoinhibition in photosystem II. *Journal of Biological Chemistry* 282: 12492–12502.
- Gründel M, Scheunemann R, Lockau W, Zilliges Y. 2012. Impaired glycogen synthesis causes metabolic overflow reactions and affects stress responses in the cyanobacterium *Synechocystis* sp. PCC 6803. *Microbiology* 158: 3032–3043.
- Haimovich-Dayan M, Kahlon S, Hihara Y, Hagemann M, Ogawa T, Ohad I, Lieman-Hurwitz J, Kaplan A. 2011. Cross-talk between photomixotrophic growth and CO₂-concentrating mechanism in *Synechocystis* sp. strain PCC 6803. *Environmental Microbiology* 13: 1767–1777.
- Heifetz PB, Fö B, Osmond CB, Giles LJ, Boynton JE. 2000. Effects of acetate on facultative autotrophy in *Chlamydomonas reinhardtii* assessed by photosynthetic measurements and stable isotope analyses 1. *Plant Physiology* 122: 1439–1445.
- Ishikita H, Galstyan A, Knapp EW. 2007. Redox potential of the non-heme iron complex in bacterial photosynthetic reaction center. *Biochimica et Biophysica Acta – Bioenergetics* 1767: 1300–1309.
- Johnson VM, Pakrasi HB. 2022. Advances in the understanding of the lifecycle of photosystem II. *Microorganisms* 10: 1–19.
- Kahlon S, Beeri K, Ohkawa H, Hihara Y, Murik O, Suzuki I, Ogawa T, Kaplan A. 2006. A putative sensor kinase, Hik31, is involved in the response of *Synechocystis* sp. strain PCC 6803 to the presence of glucose. *Microbiology* 152: 647–655.
- Kanno M, Carroll AL, Atsumi S. 2017. Global metabolic rewiring for improved CO₂ fixation and chemical production in cyanobacteria. *Nature Communications* 8: 14724.
- Latifi A, Ruiz M, Zhang CC. 2009. Oxidative stress in cyanobacteria. *FEMS Microbiology Reviews* 33: 258–278.
- Lea-Smith DJ, Bombelli P, Vasudevan R, Howe CJ. 2016. Photosynthetic, respiratory and extracellular electron transport pathways in cyanobacteria. *Biochimica et Biophysica Acta (BBA) – Bioenergetics* 1857: 247–255.
- Lee HW, Park BS, Joo JH, Patidar SK, Choi HJ, Jin ES, Han MS. 2018. Cyanobacteria-specific algicidal mechanism of bioinspired naphthoquinone derivative, NQ 2-0. *Scientific Reports* 8: 11595.
- Lee S, Ryu JY, Soo YK, Jeon JH, Ji YS, Cho HT, Choi SB, Choi D, De Marsac NT, Il PY. 2007. Transcriptional regulation of the respiratory genes in the cyanobacterium *Synechocystis* sp. PCC 6803 during the early response to glucose feeding. *Plant Physiology* 145: 1018–1030.
- Luan G, Zhang S, Wang M, Lu X. 2019. Progress and perspective on cyanobacterial glycogen metabolism engineering. *Biotechnology Advances* 37: 771–786.

- Makowka A, Nichelmann L, Schulze D, Spengler K, Wittmann C, Forchhammer K, Gutekunst K. 2020. Glycolytic shunts replenish the Calvin–Benson–Bassham cycle as anaplerotic reactions in cyanobacteria. *Molecular Plant* 13: 471–482.
- Mallen-Ponce MJ, María Esther Perez-Perez MP, Crespo JL. 2022. Photosynthetic assimilation of CO₂ regulates TOR activity. *Proceedings of the National Academy of Sciences, USA* 119: e2115261119.
- Markwell MAK, Haas SM, Bieber LL, Tolbert NE. 1978. A modification of the lowry procedure to simplify protein determination in membrane and lipoprotein sample. *Analytical Biochemistry* 87: 206–210.
- Matson MM, Atsumi S. 2018. Photomixotrophic chemical production in cyanobacteria. *Current Opinion in Biotechnology* 50: 65–71.
- Miller NT, Ajlani G, Burnap RL. 2022. Cyclic electron flow-coupled proton pumping in *Synechocystis* sp. PCC6803 is dependent upon NADPH oxidation by the soluble isoform of Ferredoxin:NADP-Oxidoreductase. *Microorganisms* 10: 855.
- Mullineaux CW. 2014. Co-existence of photosynthetic and respiratory activities in cyanobacterial thylakoid membranes. *Biochimica et Biophysica Acta (BBA) – Bioenergetics* 1837: 503–511.
- Muñoz-Marín MDC, López-Lozano A, Moreno-Cabezuelo JÁ, Díez J, García-Fernández JM. 2024. Mixotrophy in cyanobacteria. *Current Opinion in Microbiology* 78: 102432.
- Murata N, Takahashi S, Nishiyama Y, Allakhverdiev SI. 2007. Photoinhibition of photosystem II under environmental stress. *Biochimica et Biophysica Acta (BBA) – Bioenergetics* 1767: 414–421.
- Muth-Pawlak D, Kreula S, Gollan PJ, Huokko T, Allahverdiyeva Y, Aro EM. 2022. Patterning of the autotrophic, mixotrophic, and heterotrophic proteomes of oxygen-evolving cyanobacterium *Synechocystis* sp. PCC 6803. *Frontiers in Microbiology* 13: 891895.
- Nakajima T, Kajihata S, Yoshikawa K, Matsuda F, Furusawa C, Hirasawa T, Shimizu H. 2014. Integrated metabolic flux and omics analysis of *Synechocystis* sp. PCC 6803 under mixotrophic and photoheterotrophic conditions. *Plant and Cell Physiology* 55: 1606–1612.
- Nikkanen L, Santana Sánchez A, Ermakova M, Rögner M, Cournac L, Allahverdiyeva Y. 2020. Functional redundancy between flavodiiron proteins and NDH-1 in *Synechocystis* sp. PCC 6803. *The Plant Journal* 103: 1460–1476.
- Nikkanen L, Solymosi D, Jokel M, Allahverdiyeva Y. 2021. Regulatory electron transport pathways of photosynthesis in cyanobacteria and microalgae: recent advances and biotechnological prospects. *Physiologia Plantarum* 173: 514–525.
- Ogawa T, Sonoike K. 2016. Effects of bleaching by nitrogen deficiency on the quantum yield of Photosystem II in *Synechocystis* sp. PCC 6803 revealed by Chl fluorescence measurements. *Plant and Cell Physiology* 57: 558–567.
- Ogawa T, Suzuki K, Sonoike K. 2021. Respiration interacts with photosynthesis through the acceptor side of photosystem I, reflected in the dark-to-light induction kinetics of chlorophyll fluorescence in the cyanobacterium *Synechocystis* sp. PCC 6803. *Frontiers in Plant Science* 12: 717968.
- Ortega-Martínez P, Roldán M, Díaz-Troya S, Florencio FJ. 2023. Stress response requires an efficient connection between glycogen and central carbon metabolism by phosphoglucosyltransferases in cyanobacteria. *Journal of Experimental Botany* 74: 1532–1550.
- Rippka R, Deruelles J, Waterbury JB, Herdman M, Stanier RY. 1979. Generic assignments, strain histories and properties of pure cultures of cyanobacteria. *Microbiology* 111: 1–61.
- Roach T, Sedoud A, Krieger-Liszka A. 2013. Acetate in mixotrophic growth medium affects photosystem II in *Chlamydomonas reinhardtii* and protects against photoinhibition. *Biochimica et Biophysica Acta – Bioenergetics* 1827: 1183–1190.
- Rodríguez-Gil T, Torrado A, Iniesta-Pallarés M, Álvarez C, Mariscal V, Molina-Heredia FP. 2021. Cytochrome *c_m* is probably a membrane protein similar to the C subunit of the bacterial nitric oxide reductase. *Applied Sciences* 11: 9396.
- Schreiber U, Klughammer C. 2016. Analysis of photosystem I donor and acceptor sides with a new type of online-deconvoluting kinetic LED-array spectrophotometer. *Plant and Cell Physiology* 57: 1454–1467.
- Schuller JM, Birrell JA, Tanaka H, Konuma T, Wulffhorst H, Cox N, Schuller SK, Thiemann J, Lubitz W, Séfif P *et al.* 2019. Structural adaptations of photosynthetic complex I enable ferredoxin-dependent electron transfer. *Science* 363: 257–260.
- Schulze D, Kohlstedt M, Becker J, Cahoreau E, Peyriga L, Makowka A, Hildebrandt S, Gutekunst K, Portais JC, Wittmann C. 2022. GC/MS-based 13C metabolic flux analysis resolves the parallel and cyclic photomixotrophic metabolism of *Synechocystis* sp. PCC 6803 and selected deletion mutants including the Entner-Doudoroff and phosphoketolase pathways. *Microbial Cell Factories* 21: 69.
- Shevela D, Klimov V, Messinger J. 2007. Interactions of photosystem II with bicarbonate, formate and acetate. *Photosynthesis Research* 94: 247–264.
- Shi LX, Hall M, Funk C, Schröder WP. 2012. Photosystem II, a growing complex: updates on newly discovered components and low molecular mass proteins. *Biochimica et Biophysica Acta – Bioenergetics* 1817: 13–25.
- Solymosi D, Nikkanen L, Muth-Pawlak D, Fitzpatrick D, Vasudevan R, Howe CJ, Lea-Smith DJ, Allahverdiyeva Y. 2020. Cytochrome *c_m* decreases photosynthesis under photomixotrophy in *Synechocystis* sp. PCC 6803. *Plant Physiology* 183: 700–716.
- Solymosi D, Shevela D, Allahverdiyeva Y. 2022. Nitric oxide represses photosystem II and NDH-1 in the cyanobacterium *Synechocystis* sp. PCC 6803. *Biochimica et Biophysica Acta – Bioenergetics (BBA)* 1863: 148507.
- Sun Z, Zhao X, Li G, Yang J, Chen Y, Xia M, Hwang I, Hou H. 2023. Metabolic flexibility during a trophic transition reveals the phenotypic plasticity of greater duckweed (*Spirodela polyrrhiza* 7498). *New Phytologist* 238: 1386–1402.
- Theune ML, Hildebrandt S, Steffen-Heins A, Bilger W, Gutekunst K, Appel J. 2021. *In-vivo* quantification of electron flow through photosystem I – cyclic electron transport makes up about 35% in a cyanobacterium. *Biochimica et Biophysica Acta – Bioenergetics* 1862: 148353.
- Thiel K, Vuorio E, Aro EM, Kallio PT. 2017. The effect of enhanced acetate influx on *Synechocystis* sp. PCC 6803 metabolism. *Microbial Cell Factories* 16: 21.
- Trautmann D, Voß B, Wilde A, Al-Babili S, Hess WR. 2012. Microevolution in cyanobacteria: re-sequencing a motile substrain of *Synechocystis* sp. PCC 6803. *DNA Research* 19: 435–448.
- Vass I, Kirilovsky D, Etienne AL. 1999. UV-B radiation-induced donor- and acceptor-side modifications of photosystem II in the cyanobacterium *Synechocystis* sp. PCC 6803. *Biochemistry* 38: 12786–12794.
- Wan N, Abernathy M, Tang JKH, Tang YJ, You L. 2015. Cyanobacterial photo-driven mixotrophic metabolism and its advantages for biosynthesis. *Frontiers of Chemical Science and Engineering* 9: 308–316.
- Wang Y, Chen X, Spengler K, Terberger K, Boehm M, Appel J, Barske T, Timm S, Battchikova N, Hagemann M *et al.* 2022. Pyruvate : ferredoxin oxidoreductase and low abundant ferredoxins support aerobic photomixotrophic growth in cyanobacteria. *eLife* 11: e71339.
- Wydrzynski T, Govindjee. 1975. A new site of bicarbonate effect in photosystem II of photosynthesis: evidence from chlorophyll fluorescence transients in spinach chloroplasts. *Biochimica et Biophysica Acta* 387: 403–408.
- Yamada M, Nagao R, Iwai M, Arai Y, Makita A, Ohta H, Tomo T. 2018. The PsbQ' protein affects the redox potential of the *Q_A* in photosystem II. *Photosynthetic* 56: 185–191.
- Yoshikawa K, Hirasawa T, Ogawa K, Hidaka Y, Nakajima T, Furusawa C, Shimizu H. 2013. Integrated transcriptomic and metabolomic analysis of the central metabolism of *Synechocystis* sp. PCC 6803 under different trophic conditions. *Biotechnology Journal* 8: 571–580.
- Zavřel T, Očenašová P, Červený J. 2017. Phenotypic characterization of *Synechocystis* sp. PCC 6803 substrains reveals differences in sensitivity to abiotic stress. *PLoS ONE* 12: e0189130.

Supporting Information

Additional Supporting Information may be found online in the Supporting Information section at the end of the article.

Dataset S1 Quantification of metabolites in WT, ΔPGM and ΔAGP *Synechocystis* strains after glucose addition.

Fig. S1 Measurements of enzymatic activities at the glucose-6P metabolic crossroads in WT, Δ PGM and Δ AGP *Synechocystis* cell extracts.

Fig. S2 Effect of glucose on the photosynthetic machinery integrity in WT, Δ PGM and Δ AGP *Synechocystis* strains.

Fig. S3 Growth recovery of WT, Δ PGM and Δ AGP *Synechocystis* strains after glucose removal from the media.

Fig. S4 Time course metabolic profile extension.

Fig. S5 Comparison of metabolite levels under autotrophy and 30 min after glucose addition to WT, Δ PGM and Δ AGP *Synechocystis* cultures.

Fig. S6 Quantification of CO₂ fluxes in WT, Δ PGM and Δ AGP *Synechocystis* strains before and 30 min after glucose supplementation.

Fig. S7 Photosystems abundance ratio in photoautotrophy and 30 min after glucose addition to WT, Δ PGM and Δ AGP *Synechocystis* strains.

Fig. S8 Analysis of the effect of glucose on the PSII effective yield in WT, Δ PGM and Δ AGP *Synechocystis* strains.

Fig. S9 Measurements of O₂ fluxes in MIMS in WT, Δ PGM and Δ AGP *Synechocystis* strains.

Fig. S10 Real-time effects of glucose addition on oxygen evolution and CO₂ uptake in Δ AGP cultures determined by MIMS.

Fig. S11 Redox state changes of P700 (PSI), its donor side Plastocyanin and its acceptor side Ferredoxin in photoautotrophy and 30 min after glucose addition to WT, Δ PGM and Δ AGP *Synechocystis* cultures.

Methods S1 Enzyme activity assays.

Methods S2 Photosystems abundance ratio.

Please note: Wiley is not responsible for the content or functionality of any Supporting Information supplied by the authors. Any queries (other than missing material) should be directed to the *New Phytologist* Central Office.